Elsevier Editorial System(tm) for Journal of Hydrology

Manuscript Draft

Manuscript Number: HYDROL14331R1

Title: Modelling of sediment transport and bed deformation in rivers with continuous bends

Article Type: Research Paper

Keywords: RNG k-ε turbulence model, bed deformation, suspended sediment, bedload sediment, bed material granularity

Corresponding Author: Dr. Hefang Jing, Ph.D.

Corresponding Author's Institution: Beifang University of Nationalities

First Author: Hefang Jing, Ph.D.

Order of Authors: Hefang Jing, Ph.D.; Chunguang Li, Ph.D.; Yakun Guo, Ph.D.; Lixiang Zhang; Lijun Zhu; Yitian Li, Ph.D.

Dr Hefang Jing

Research Institute of Numerical Computation & Engineering Applications
Beifang University of Nationalities
Yinchuan 750021
Email: jinghef@163.com
P.R. China

5 May, 2013

Dr. Andras Bardossy
Editorial Coordinator
Journal of Hydrology

Dear Dr. Bardossy:

Re: Modeling of sediment transport and bed deformation in rivers with continuous bends

Authors: Hefang Jing, Chunguang Li, Yakun Guo, Lixiang Zhang and Lijun Zhu and Yitian Li
Manuscript No: HYDROL14331

Please find attached revision of the above manuscript and the detailed response to the comments/suggestions made by the Editor and two Reviewers. You can see from the revised manuscript and the point-to-point response that we have fully considered and adequately addressed all the comments made by reviewers. We hope that the revised manuscript is now suitable for the publication in *Journal of Hydrology* as a research paper. In editing the revised manuscript, Professor Yitian Li, Wuhan University, has made a significant contribution to the revision. Therefore, we all agree to include Prof. Li as a co-author of the paper.

Should you need to contact me, please use the above address or contact me by fax at:

++86 951 2068011 or via Email shown above.

I am looking forward to hearing from you.

Yours sincerely,

Dr Hefang Jing

Highlights

Title：Modelling of sediment transport and bed deformation in rivers with continuous bends

1. We improve a 2D RNG k-ε sediment model including the effect of secondary currents.
2. We develop an efficient semi-coupled scheme to solve sediment models numerically.
3. Bed deformation induced by transport of non-uniform suspended and non-uniform bedload sediments is investigated.
4. The variation of effective bed material granularity has been examined.

Responses

Title: Modelling of sediment transport and bed deformation in rivers with continuous bends
Authors: Hefang Jing, Chunguang Li, Yakun Guo, Lixiang Zhang, Lijun Zhu, Yitian Li.
Manuscript No: #HYDROL14331

The Editor

General comment: The authors should sincerely address the comments by the reviewers before it can be considered for its possible publication in J of Hydrology. The revised paper will be sent to the reviewers to check if their comments are well addressed.

Response: The authors are very grateful for the comments and suggestions made by the Editor and two reviewers. The authors have fully considered and addressed these comments in the revised manuscript which has been rewritten. They hope that the revised manuscript is now suitable for publication in Journal of Hydrology as a Research Article.

Comments of Reviewers

Reviewer #2

Comments to the Author

General comment: In summary, this is a case-study paper that applied 2D depth-averaged model to simulate sediment transport in river meanders. There is no considerable contribution to the 2D modeling research. This paper is a repeated work of other published papers. The only difference is the implementation of RNG k-e model, which may not be necessary for a 2D depth-averaged model. This is an excellent case study paper that can be published in conference proceedings, or ASCE journal's case study paper.

General response: The authors appreciate the comments made by this Reviewer. First, the proposed numerical method is generic and can be used for simulating any natural rivers with bends instead of a case study. The proposed semi-coupled scheme can be used to efficiently solve most of sediment models, including 1D, 2D and 3D sediment models. The main reasons that the authors choose the upper reach of the Yellow river are (1) the reach under investigation is a typical representative natural river reach having several continuous bends and is famous for its sediment transport; and (2) some detailed flow and sediment transport measurements are available in the reach

which can be used for validating the model. Second, for the problem under investigation, the authors think that the RNG *k*-*ε* model is necessary. The reason is as following (also stated in the MS). In the simulation of the studied reach, other mathematical models, such as laminar flow model, one equation model, standard *k*-*ε* model, have been applied, but the results are poorly compared with the field measurements as these models can't simulate the effect of the secondary currents on the flow and sediment transport. So the authors developed the 2D RNG *k*-*ε* turbulent sediment model, in which the effect of the secondary currents is considered. Finally, as for the contribution, the proposed semi-coupled scheme can obtain the similar accurate results as coupled model but the computational cost is significantly reduced. Therefore, the authors consider this is one significant contribution. The modified RNG *k*-*ε* model is another contribution to the river flow models.

Comment 1. (line 11, page 1) delete "the". Please check the use of "the" throughout the manuscript.

Response 1. The authors thank the reviewer for pointing out this mistake which has been corrected. Careful proof reading has been carried out to eliminate any possible errors/mistakes throughout the manuscript.

Comment 2. (page 2, line 25-38) This part about 1D, 2D and 3D model description is biased. Please note it's well known 1D, 2D, and 3D models can be used to simulate flow and sediment transport. There is no need to explain why 2D model is needed. The authors should delete this paragraph.

Response 2. The authors are grateful for this suggestion. The paragraph is deleted according to the reviewer's suggestion.

Comment 3. (Page 3: line 55-60) Please comments on those models, and indicate clearly what has not been achieved in 2D models. Why are those 2D models not enough in literature? What are new in your 2D model?

Response3. The authors thank the reviewer for these suggestions. The relevant paragraph has been rewritten with the appropriate comments on existing 2D models and the proposed 2D model in this study (for details, please see Page 3-4: Line 48-70 in revised manuscript).

Comment 4.(Page 4, line 75)
The RNG k-e model is developed primarily for 3D RANS model. Applying the depth-averaged version of RNG k-e model in 2D model doesn't seem to improve the solution of turbulence flow field comparing to other simple turbulence closures, such as parabolic, standard k-e model.

Response4. The reviewer is correct that the RNG *k*-*ε* model is developed from 3D

standard k-ε model. Compared with the standard k-ε model and parabolic model, however, the RNG k-ε model has following advantages which have been confirmed in this study:

(1) The computational accuracy of the RNG k-ε model is higher than that of the standard k-ε model/parabolic model due to an extra term being added in the ε-equation of the RNG k-ε model;
(2) The model can be used to simulate the turbulent eddy with high accuracy of which the standard k-ε model or parabolic model can't achieve;
(3) The model can be applied to simulate both the high and low Reynolds number flows;
(4) The computational cost of the model is comparable with that of the standard k-ε model/parabolic (only about 10%~15% more CPU time required) while the simulation accuracy is much higher than that of the standard k-ε model/parabolic model.

In summary, the RNG k-ε model is more accurate and has more extensive application than standard k-ε model/parabolic model. This is why the authors choose the 3D RNG k-ε model to develop 2D depth averaged RNG k-ε model in which some parameters have been modified and extra source terms have been added to the momentum equations in order to simulate the effect of the secondary currents on the main flow field and sediment transport. In order to illustrate this, In Figure 5(1), comparison is presented from the numerical results of considering and without considering the effect of secondary currents.

Comment 5. (Page 4, line 80-81) This description is hard to understand. Please note "coupled" means the governing equations are solved simultaneously, while decoupled means solved separately. What does "semi-coupled' mean?

Response 5. The authors are grateful for this comment. In the revised version, the authors have explained "coupled", "decoupled" and semi-coupled" in detail (Page 4-6, Line 72-99). In this study, the coupled scheme means that the hydraulic and sediment modules are working every time step. However, at every time step, hydraulic module is solved first, then the sediment module. In the decoupled scheme, the hydraulic module has been run first alone for a certain number of time steps until the prescribed computational accuracy is achieved. The sediment module then starts to run alone until the prescribed computational accuracy is achieved. In the semi-coupled scheme, the hydraulic module does not keep running all the time as the coupled scheme does, while it does not also keep shutting after some time steps as the decoupled scheme does. In the semi-coupled scheme, the hydraulic module runs intermittently in order to update the flow field as well as to reduce the computational cost.

Comment 6. (Page 4, line 86) "Plane" should be "depth-averaged"

Response 6. The good suggestion has been adopted throughout the revised manuscript with thanks.

Comment 7. (Page 5, line 103-105) please make sure the symbols are aligned well with text.

Response 7. The symbols have been adjusted to be aligned well with text according to the suggestion with thanks.(see Page 7: Line 118-127).

Comment 8. (Page 6, line 124) I don't see the values by converting the governing equations to the body-fitted coordinates. As well known, there are many additional terms that make the solution of 2D depth-averaged momentum equations complex.

Response 8. The authors thank the reviewer for this comment. It is true that the governing equations in the body-fitted coordinates are a little more complex than those in Cartesian coordinates. The main reason or advantage of using body-fitted coordinates system is to better fit the very complex computational domain. Using body-fitted coordinates system, the complex physical area is converted to a simple regular computational domain which enables a much easier discretisation. Furthermore, in body-fitted coordinates system we can make grid line accordance with streamline, which can reduce the error of numerical schemes.

Comment 9. (Page 8 line 177) Zhang (1988) equation is an empirical based sediment rating curve for the Lower Yellow River.

Response 9. The Reviewer is correct about this empirical formula. The authors have tested a few formulas and found that this formula gave the best simulation results.

Comment 10. (Line 213-216) It's necessary to write out the discretized equations, especially how the RNG k-e models are discretized unless the discretized equations have been published in other papers.

Response 10. The Reviewer is thanked for pointing out this missing information. The discretized equations and the associated text have been added in the revised manuscript (see Page 12-15: line 221-276 in the revised version).

Comment 11. (Line 219-225)This is not completely true because when decoupled scheme is used, the bed elevation change at each time step has minimal impacts on flow field. If bed changes are too rapid, it's necessary to use coupled scheme, but for a long-term simulation (the advantages of 2D model), decoupled scheme is more efficient.

Response 11. The authors are grateful for this comment and suggestion. The relevant text has been modified accordingly with thanks (see Page 4-6: Line 72-99; Page 15-16: Line 284-298 in the revised version).

Comment 12. (Line 238) In fact, the authors' "semi-coupled" scheme is the decoupled scheme in which flow and sediment have different time steps.

Response 12. In fact, the proposed semi-coupled scheme is different from the decoupled scheme. In the decoupled scheme, the flow module will stop running forever when the sediment module begins to run; while in the semi-coupled scheme proposed in this study, after sediment module begins to run, the flow module will still run intermittently, though not continuously. In the semi-coupled scheme, when the flow and sediment modules are running, they have the same time step. The sleeping time interval of flow module every time usually is very long (e.g.12h), depending on the bed change condition. However, we cannot set the time step of flow as 12h, which is unreasonable.

Reviewer #3:

Comment 1. (PAGE 09, LINE 146) please index your nomenclature of parameters.

Response 1. The authors are grateful for such good suggestion. The nomenclature of parameters has been added in the revised manuscript (see Page 2 in the revised version)

Comment 2. (PAGE 12, LINE 204): please verify details of discretization for time domain and space domain, separately.

Response 2. The Reviewer is thanked for pointing out this missing information. The details of the discretization process for both the temporal and spatial domain have been added in the revision (see Page 12-15: Line 221-276 in the revised version).

Comment 3. (PAGE 13, LINE 218) please clarify the meaning of semi-coupled algorithm and necessity of such nomination.

Response 3. This comment is similar to the comments 5 and 12 made by the Reviewer #2. In the revised version, the authors have provided the explanation of the meaning of semi-coupled scheme (algorithm) and the necessity of such nomination. (see Page 4-6: Line 72-99; Page 15-16: Line 284-309 in the revised version).

Comment 4. (PAGE 14, LINE 230) please clarify each of 'coupled' and 'separate' algorithms.

Response 4. The comment is related to above comment as well as the comments 5 and 12 made by the Reviewer #2. Details of the “coupled” and “separated”(decoupled) algorithm(scheme) have been added in the revision with thanks (see Page 4-6: line 72-99; Page 15-16: line 284-309 in the revised version).

Comment 5. (PAGE 17, LINE 296) please discuss on mesh density and uniformity or non-uniformity of mesh distribution.

Response 5. The Reviewer is thanked for this very good suggestion. The flow field changes dramatically near solid wall boundary and bend, so the mesh density near river banks and bends is greater than other positions. Relevant text about the mesh density and distribution has been added in the revision and a new figure (Figure 2 in the revised version) to clearly demonstrate the mesh density and distribution in the computational domain.

Comment 6. (PAGE 20, LINE 361) please extol configuration modality of your figures.

Response 6. The authors thank the reviewer for this suggestion. Some figures with low quality are improved (Figure 4 in the revise version) or replaced with table (Figure 1 in the origin version is replaced with Table 2 in the revised version) in the revision.

Comment 7. (PAGE 20, LINE 369) based on the line 278,"The initial values are based on field measured data on December 6, 2008" for Boundary and initial conditions, and based on the line 371, "the simulated bed elevation along the longitudinal direction is compared with field data measured on July 17 2009", please clarify this time space.

Response 7. The authors are grateful for such suggestion. The authors had conducted two field measurements from December 6, 2008 to July 17, 2009. The time space is 203 days. The initial condition is based on the data measured on December 6, 2008, and boundary condition is linearly interpolated by the data measured on December 6, 2008 and the data measured on July 17, 2009. In the revised version, the authors have emphasized the above information (see Page 16:Line 312-321 in the revised version).

Comment 8. (PAGE 25, LINE 471) please clarify the range of small discharge at the inlet.

Response 8. The reviewer is thanked for pointing out this missing information. The authors have carefully checked the manuscript and clarified the range of small discharge (see Page 27: line 547 in the revised version).

Comment 9. (PAGE 25, LINE 475) please check substituting "material granularity" with "material composition" in line 475.

Response 9. The authors are very grateful for this suggestion which has been adopted throughout the revised manuscript.

Modelling of sediment transport and bed deformation in rivers with continuous bends*

Hefang Jing[a†] *Chunguang Li*[a] *Yakun Guo*[b] *Lixiang Zhang*[c] *Lijun Zhu*[d] *Yitian Li*[e]

[a] Res. Inst. Numer. Comput. & Eng. Appl., Beifang University of Nationalities, Yinchuan 750021, China.
[b] School of Engineering, University of Aberdeen, Aberdeen, AB24 3UE, UK.
[c] Department of Engineering Mechanics, Kunming University of Science and Technology, Kunming, 650051, China.
[d] School of Information and Computing Science, Beifang University of Nationalities, Yinchuan 750021, China.
[e] State Key Laboratory of Water Resources and Hydropower Engineering Sciences, Wuhan University, Wuhan 430072, China.

Abstract

A two dimensional (2D) RNG *k-ε* sediment model including the effects of secondary currents is developed to simulate sediment transport and bed deformation in rivers with continuous bends. Nonuniform suspended and bedload sediment transports and variation of effective bed material size distribution are included in the model. A semi-coupled scheme for sediment model is proposed, which can be used for simulating both the long- and short-term sediment transport whenever riverbed changes. The model is applied to simulate the flow and sediment transport in the Shapotou reservoir in the upper reach of the Yellow River which is a typical natural river reach with continuous bends. River bed deformations caused by suspended and bedload sediment transport are investigated. Good agreement between the numerically simulated results and the field measurements is obtained, indicating that the model is capable of simulating the sediment transport and predicting the bed deformation of rivers having continuous bends with reasonable accuracy.

Key words：RNG *k-ε* turbulence model, bed deformation ，suspended sediment, bedload sediment,

* **Grant sponsor:** the Major Research Plan Project, National Natural Science Foundation of China (grant number: 91230111 and 51279071); National Key Basic Research Development Program of China (973 Program, grant number: 2010CB429002); Project of Science and Technology of Colleges in Ningxia, China (grant number: NGY2012097); Project of Beifang University of Nationalities, China (grant number: 2012XZK05); Foreign Expert Project of Beifang University of Nationalites, China.

† Address for Correspondence: Dr. Hefang Jing, Res. Inst. Numer. Comput. & Eng. Appl., Beifang University of Nationalities, Yinchuan 750021, China. Email: jinghef@163.com. Tel: +86 951 2068011

bed material granularity

NOMENCLATURE

C	Chezy coefficient	h	water depth
D_{50}	medium diameter of bed material	k	turbulent kinetic energy
P_{mL}	bed material granularity	n	Manning coefficient
$P_{mL,0}$	original bed material granularity	u	velocity in x direction
S	sediment concentration	v	velocity in y direction
S_L	group sediment concentration	z	water level
S_v	sediment concentration by volume	α_L	group saturation recovery coefficient of sediment
S^*	sediment carrying capacity	γ	water specific gravity
S_L^*	group sediment carrying capacity	γ'	dry specific gravity of sediment
$\overline{U}$	depth averaged velocity	κ	Karman constant
Z	bed elevation	ε	turbulence dissipation rate
$Z_{S,L}$	the deposition thickness of the L-th group suspended sediment	ν	water viscosity
$Z_{b,L}$	the deposition thickness of the L-th group bedload	ν_t	water eddy viscosity
d_{50}	medium diameter of suspended sediment	γ_s	sediment specific gravity
d_m	averaged diameter of suspended sediment	γ_m	Specific gravity of muddy water
d	diameter of sediment	ω	sediment settling velocity
g	gravity acceleration	ω_L	sediment settling velocity of the L-th group sediment

1. Introduction

Flow and sediment transport near hydraulic structures in rivers have been extensively studied using various approaches, such as theoretical analysis, laboratory experiments, field measurements and numerical simulation. Among these approaches, numerical simulation has advantages in several aspects and has been increasingly used (Falconer 1992; Guo *et al.* 2007). In natural rivers,

horizontal scale is usually much greater than vertical scale; therefore, it is suitable to apply depth averaged 2D models (Guo *et al.* 2012). Generally speaking, numerical simulation using these models not only requires less computational time than three dimensional (3D) sediment models (particularly for large scale simulation), but also is more accurate than that of one dimensional (1D) sediment models. As a result, depth averaged 2D sediment models are widely applied in engineering to study sediment transport and river bed deformation. Nagata *et al.* (2000) developed a 2D sediment model for inviscid river banks. Hung *et al.* (2009) developed an unsteady 2D depth-averaged model for nonuniform sediment transport in alluvial channels, taking the transport mechanisms of cohesive and noncohesive sediment, suspended sediment and bedload into account. Duan and Julien (2010) conducted 2D numerical simulation for a laboratory bend, considering transport of suspended sediment and bedload, and river bed deformation. Li and Millar (2011) developed a 2D morphodynamic model of gravel-bed river with floodplain vegetation, considering the effects of riparian and floodplain vegetation on bank strength, floodplain flow resistance, shear stress partitioning, and bedload transport. Serrano-Pacheco *et al.* (2012) conducted 2D bedload transport simulations, in which bedload transport is governed by a power law of flow velocity and by a flow/sediment interaction parameter.

Though these 2D sediment models have been widely used to simulate the sediment transport and bed deformation in rivers and open channels, many of them are either laminar model, or zero equation turbulent model or standard k-ε turbulent model. As such, they cannot be applied to simulate the complicated turbulent flow and sediment transport in rivers with continuous bends in which the effect of secondary currents induced by the bends or curved channels is important.

Some models were modified and taken the effect of secondary currents into account, but they can only be applied to simulate the regular bends in laboratory open channels, and are difficult to be applied to simulate the flow and sediment transport in natural rivers with continuous bends under investigation. Therefore, these 2D sediment models need to be improved before they can be applied to simulate the natural rivers with continuous curves.

The RNG k-ε model, developed from standard k-ε model (Versteeg and Malalasekera,1995), has the advantages over the standard k-ε model. For example, it is more accurate by adding an extra term in the ε-equation; can be used to simulate the turbulent eddy with high accuracy and is applicable to simulate the flows of both the high and low Reynolds number (Jing et al. 2009, 2011). In this study, a 2D depth averaged RNG k-ε sediment model is developed to simulate the flow and sediment transport in the Shapotou reservoir at the upper reach of the Yellow River with continuous bends. The effect of secondary current on flow transport is taken into account in the turbulent model. Both the non-uniform suspended and non-uniform bedload sediment transport is included in the model. In addition, the variation of size distribution of effective bed materials is also simulated in the model. Depth averaged velocity, water level, transport of suspended sediment and bed deformation caused by suspended and bedload sediment transports are investigated.

The governing equations of sediment models can be divided into two modules: flow module and sediment module. The first module includes flow continuous equation, momentum equations and turbulence equations, while the second module includes transportation equations of suspended

sediment and bedload and bed deformation equations. Therefore, there are two basic schemes to numerically solve sediment models, i.e. coupled scheme and decoupled scheme. In the coupled scheme, the flow and sediment modules are solved simultaneously, while in the decoupled scheme, the flow module is solved first, then the sediment module. In other words, in the decoupled scheme, the flow module will no longer be run after the sediment module starts. Generally speaking, the coupled scheme is suitable for short time numerical simulation with the rapid change of the river bed. It is usually not suitable for long time numerical simulation of sediment transport due to the large CPU time consuming. On the other hand, the decoupled scheme is suitable for long time numerical simulation with the slow variation of river bed as it requires less computing time. Usually, the hydraulic elements, such as water level and velocity, change very slightly in the long time numerical simulation of sediment transport when river bed changes slowly. In this situation, it is not necessary to calculate the flow module every time step from the point of view of computing cost. However, after a certain time steps of running the sediment module, the river bed deformation accumulates to a degree that can significantly affect the flow elements. In this situation, the flow module needs to be run to account the effect of sediment transport and bed deformation on the flow field. However, in the decoupled scheme, the flow module is stopped forever after sediment module begins to run. Therefore, the decoupled scheme is unreasonable and needs to be improved in order to simulate the effect of the sediment transport on the flow field. This is one of the motivations of this work in which a semi-coupled scheme is developed by combining the advantages of coupled and decoupled schemes. In the proposed scheme, the sediment module keeps running, while the flow module runs intermittently. Therefore, the scheme is efficient and is less time consuming than the coupled scheme and is more accurate than the

decoupled scheme. The semi-coupled scheme is not only suitable for simulating both the long and short time sediment transport, but is also capable of treating both the rapid and slow change of the river bed.

2. Mathematical model

2.1. The 2D depth averaged RNG k-ε model in Cartesian coordinate

The 2D depth averaged RNG *k-ε* sediment model includes two basic modules: hydraulic module and sediment module. The hydraulic module consists of the following equations (Versteeg and Malalasekera, 1995; Duan and Nanda 2006; Serrano-Pacheco, *et al.* 2012):

$$\frac{\partial z}{\partial t}+\frac{\partial (hu)}{\partial x}+\frac{\partial (hv)}{\partial y}=0 \tag{1}$$

$$\frac{\partial (hu)}{\partial t}+\frac{\partial (huu)}{\partial x}+\frac{\partial (huv)}{\partial y}=\frac{\partial }{\partial x}\left(\nu_e h\frac{\partial u}{\partial x} \right)+\frac{\partial }{\partial y}\left(\nu_e h\frac{\partial u}{\partial y} \right)-gh\frac{\partial z}{\partial x}-\frac{gn^2u\sqrt{u^2+v^2}}{h^{1/3}} \tag{2}$$

$$\frac{\partial (hv)}{\partial t}+\frac{\partial (hvu)}{\partial x}+\frac{\partial (hvv)}{\partial y}=\frac{\partial }{\partial x}\left(\nu_e h\frac{\partial v}{\partial x} \right)+\frac{\partial }{\partial y}\left(\nu_e h\frac{\partial v}{y} \right)-gh\frac{\partial z}{\partial y}-\frac{gn^2v\sqrt{u^2+v^2}}{h^{1/3}} \tag{3}$$

$$\frac{\partial (hk)}{\partial t}+\frac{\partial (huk)}{\partial x}+\frac{\partial (hvk)}{\partial y}=\frac{\partial }{\partial x}\left(\alpha_k \nu_e h\frac{\partial k}{\partial x} \right)+\frac{\partial }{\partial y}\left(\alpha_k \nu_e h\frac{\partial k}{\partial y} \right)+h(P_k+P_{kv}-\varepsilon) \tag{4}$$

$$\frac{\partial (h\varepsilon)}{\partial t}+\frac{\partial (hu\varepsilon)}{\partial x}+\frac{\partial (hv\varepsilon)}{\partial y}=\frac{\partial }{\partial x}\left(\alpha_\varepsilon \nu_e h\frac{\partial \varepsilon}{\partial x} \right)+\frac{\partial }{\partial y}\left(\alpha_\varepsilon \nu_e h\frac{\partial \varepsilon}{\partial y} \right)+h\left[\frac{\varepsilon}{k}(C_{1\varepsilon}^{*}P_k-C_{2\varepsilon}\varepsilon)+P_{\varepsilon v} \right] \tag{5}$$

And the sediment module includes the following equations:

$$\frac{\partial hS_L}{\partial t}+\frac{\partial huS_L}{\partial x}+\frac{\partial hvS_L}{\partial y}=\frac{\partial }{\partial x}\left(\nu_e h\frac{\partial S_L}{\partial x} \right)+\frac{\partial }{\partial y}\left(\nu_e h\frac{\partial S_L}{\partial y} \right)-\alpha_L\omega_L(S_L-S_L^{*}) \tag{6}$$

$$\gamma_s{}'\frac{\partial Z_{S,L}}{\partial t}=\alpha_L\omega_L(S_L-S_L^{*}) \tag{7}$$

$$\gamma'_s \frac{\partial Z_{b,L}}{\partial t} + \frac{\partial g_{bx,L}}{\partial x} + \frac{\partial g_{by,L}}{\partial y} = 0 \quad (8)$$

$$\gamma'_s \frac{\partial E_m P_{mL}}{\partial t} + \alpha_L \omega_L (S_L - S_L^*) + \frac{\partial g_{bx,L}}{\partial x} + \frac{\partial g_{by,L}}{\partial y} + \gamma'_s [\varepsilon_1 P_{mL} + (1-\varepsilon_1) P_{mL,0}] \left(\frac{\partial z_b}{\partial t} - \frac{\partial E_m}{\partial t} \right) = 0 \quad (9)$$

In above equations: z=the water level; *h*=the water depth; *u*, *v*= the vertically averaged velocities in x, y directions, respectively; *t*=the time; *k*= the turbulent kinetic energy; ε =the turbulence dissipation rate; *g*=the acceleration of gravity; *n*=the Manning's coefficient; S_L, $S_L^*, \omega_L, \alpha_L$ =the *L*-th group sediment concentration, sediment carrying capacity, settling velocity, saturation recovery coefficient, respectively; $Z_{S,L}$ =the deposition thickness of the *L*-th group suspended sediment, γ_s' =the dry specific gravity of sediment; $Z_{b,L}, g_{bx,L}$ and $g_{by,L}$ =deposition thickness, discharge per unit width in x and y directions of the *L*-th group bed load, respectively; P_{mL} and $P_{mL,0}$ =bed material granularity and original bed material granularity, respectively; z_b =the bed level, E_m =the thickness of active layer; $\varepsilon_1 = 0$ (if the original river bed is scoured) or $\varepsilon_1 = 1$ (if the original river bed is deposited).

In (1)-(6), the effective viscosity (ν_e) is the sum of the viscosity of water (ν) and the eddy viscosity coefficient of water (ν_t). The values and the calculation of some coefficients such as $\nu_t, P_k, P_{kv}, P_{\varepsilon v}, C_{1\varepsilon}^*, C_\mu, \alpha_k, \alpha_\varepsilon$, can be found in (Yakhot and Orzag, 1986; Rodi 1993).

2.2. Modified 2D depth averaged RNG k-ε model in body fitted coordinates

As the river reach under investigation consists of several irregular bends where strong circulation flow exists, the 2D depth averaged RNG *k*-ε sediment model usually can not reflect the influence of such flow. Therefore, the model needs to be modified to take the influence of circulation flow

137 into account.

138

139 To facilitate the description, the general control equations of the 2D depth averaged RNG *k-ε*

140 sediment model is written in the body fitted coordinate system (BFC):

141 $$\frac{\partial}{\partial t}(h\Phi)+\frac{1}{J}\frac{\partial}{\partial \xi}(hU\Phi)+\frac{1}{J}\frac{\partial}{\partial \eta}(hV\Phi)=\frac{1}{J}\frac{\partial}{\partial \xi}(\frac{\alpha h\Gamma_{\Phi}}{J}\frac{\partial \Phi}{\partial \xi})+\frac{1}{J}\frac{\partial}{\partial \eta}(\frac{\gamma h\Gamma_{\Phi}}{J}\frac{\partial \Phi}{\partial \eta})+S_{\Phi}(\xi,\eta) \quad (10)$$

142 where general variable Φ represents 1, *u*, *v*, *k*, *ε*, S_L in (1)-(6), respectively; ξ and η = the

143 curvilinear coordinates along river bank direction and perpendicular to the river bank direction,

144 respectively; J,α,β,γ = transformation factors, $J=x_{\xi}y_{\eta}-x_{\eta}y_{\xi}$, $\alpha=x_{\eta}^2+y_{\eta}^2$,

145 $\beta=x_{\xi}x_{\eta}+y_{\xi}y_{\eta}$, $\gamma=x_{\xi}^2+y_{\xi}^2$; U and V = components of inverter velocity in ξ and η

146 directions, respectively, $U=uy_{\eta}-vx_{\eta}$, $V=-uy_{\xi}+vx_{\xi}$; Γ_{Φ} = general diffusion coefficient;

147 the source terms of the momentum equations (Eq.s (2) and (3)) are as following:

148 $$S_u=-\frac{1}{J}gh(z_{\xi}y_{\eta}-z_{\eta}y_{\xi})-\frac{1}{J}\frac{\partial}{\partial \xi}\left(\frac{\beta\Gamma_u h}{J}\frac{\partial u}{\partial \eta}\right)-\frac{1}{J}\frac{\partial}{\partial \eta}\left(\frac{\beta\Gamma_u h}{J}\frac{\partial u}{\partial \xi}\right)-\frac{gn^2u\sqrt{u^2+v^2}}{h^{1/3}} \quad (11)$$

149 $$S_v=-\frac{1}{J}gh(-z_{\xi}x_{\eta}+z_{\eta}x_{\xi})-\frac{1}{J}\frac{\partial}{\partial \xi}\left(\frac{\beta\Gamma_v h}{J}\frac{\partial v}{\partial \eta}\right)-\frac{1}{J}\frac{\partial}{\partial \eta}\left(\frac{\beta\Gamma_v h}{J}\frac{\partial v}{\partial \xi}\right)-\frac{gn^2v\sqrt{u^2+v^2}}{H^{\frac{1}{3}}} \quad (12)$$

150 To simulate the influence of circulation flow of bend, extra source terms need to be added in the

151 momentum equations. These new source terms are as following (Lien, et al, 1999):

152 $$S_u^{new}=S_u+M_u \ , \ S_v^{new}=S_v+M_v \quad (13)$$

153 in which the extra source terms can be calculated by

154 $$M_u=-\frac{1}{J^2}\frac{u\sqrt{\gamma}}{\sqrt{u^2+v^2}}\frac{\partial}{\partial \eta}\left(|\bar{u}|\bar{u}\phi\right) \ , \ M_v=-\frac{1}{J^2}\frac{v\sqrt{\gamma}}{\sqrt{u^2+v^2}}\frac{\partial}{\partial \eta}\left(|\bar{u}|\bar{u}\phi\right) \quad (14)$$

155 where $\phi=\sqrt{\frac{\gamma}{\alpha}}\frac{h^2}{R_{\eta}}k_{TS}$, $\bar{u}=\frac{ux_{\xi}+vy_{\xi}}{\sqrt{\gamma}}$, $\bar{v}=\frac{ux_{\eta}+vy_{\eta}}{\sqrt{\alpha}}$, R_{η} = the curvature radius of river

156 bend, k_{TS}= the lateral exchange coefficient due to circulation flow and can be calculated by

157 $$k_{TS} = 5\frac{\sqrt{g}}{\kappa C} - 15.6\left(\frac{\sqrt{g}}{\kappa C}\right)^2 + 37.5\left(\frac{\sqrt{g}}{\kappa C}\right)^3 \quad (15)$$

158 where κ = Karman constant which is related to the sediment concentration (see below), C =
159 Chezy coefficient.

160 $$\kappa = 0.4[1 - 4.2(0.365\text{-}S_v)\sqrt{S_v}] \quad (16)$$

161 where S_v =the sediment concentration by volume.

162

163 The following key parameters need to be determined before the model can be applied for
164 simulation. .

165

166 ***2.3. Suspended sediment carrying capacity***

167 Considering the effect of sediment concentration on Karman constant and silt deposition, Zhang
168 and Zhang（1992）presented a semi-empirical and semi-theoretical formula to calculate suspended
169 sediment carrying capacity based on the relationship between energy consumption of flow and the
170 power require to float sediment. Being verified by broad range of measured data in the Yellow
171 River, the formula has a high adaptability and can be used in the Upper Yellow River. The total
172 suspended sediment carrying capacity can be calculated as following:

173 $$S^* = 2.5\left[\frac{(0.0022 + S_v)\overline{U}^3}{\kappa\frac{\gamma_s - \gamma_m}{\gamma_m} gh\omega_s}\ln\left(\frac{h}{6D_{50}}\right)\right]^{0.62} \quad (17)$$

174 where $\overline{U}$ =vertical mean velocity; D_{50}= medium diameter of bed material; γ_s, γ_m =specific
175 gravity of sediment and muddy water, respectively; ω_s =group setting velocity. The units system
176 adopted is kg, m and s.

177

178 The group sediment carrying capacity S_L^* is obtained by multiplying S^* with p_L^* (the

179 graduation of group sediment carrying capacity):

180 $$S_L^* = p_L^* S^* \tag{18}$$

181 and p_L^* can be calculated by (Zhang, 1988):

182 $$p_L^* = wp_L + (1-w)p_{bL}^{'} \tag{19}$$

183 where P_L=graduation of suspended sediment at inlet; $p_{bL}^{'}$ =related to the graduation of bed

184 material; w=weight factor, and its value ranges from 0.62 to 0.85 when the river bed is silted; from

185 0.64 to 0.86 when the river bed is scoured; and from 0.49 to 0.52 when the river bed keeps the

186 balance of erosion and deposition.

187

188 ***2.4. Sediment setting velocity***

189 The sediment setting velocity is a very important parameter in the sediment model. There are a lot

190 of formulae to calculate sediment setting velocity, among which the formula developed by Zhang

191 (1988) is one of the most representative formulae that are suitable for the sediment in the Yellow

192 River. According to Zhang (1988), the single grain sediment setting velocity in clean water can be

193 calculated as:

194 $$\omega_0 = \begin{cases} \dfrac{1}{25.6}\dfrac{\gamma_s-\gamma}{\gamma} g \dfrac{d^2}{\nu}, & \text{for } d \le 0.1\text{mm} \\ 1.044\sqrt{\dfrac{\gamma_s-\gamma}{\gamma} gd}, & \text{for } d \ge 4\text{mm} \\ \sqrt{\left(13.95\dfrac{\nu}{d}\right)^2 + 1.09\dfrac{\gamma_s-\gamma}{\gamma} gd} - C_1\dfrac{\nu}{d}, & \text{for } 0.1\text{mm} < d < 4\text{mm} \end{cases} \tag{20}$$

195 where ω_0 = the sediment setting velocity in clear water, d = the diameter of single grain sediment.

196

197 The sediment concentration in the Yellow River is usually high, which will affect the sediment
198 setting velocity. Therefore, the formula must be modified to take the effect of sediment
199 concentration into account. According to Zhang and Zhang (1992), the sediment setting velocity in
200 muddy water can be estimated as:

201 $$\omega = \omega_0 \left[\left(1 - \frac{S_v}{2.25\sqrt{d_{50}}} \right)^{3.5} (1 - 1.25 S_v) \right] \tag{21}$$

202 where d_{50} is the medium diameter of a group of sediment.

203

204 ***2.5. Bedload sediment transport rate***

205 Bedload transport rate is an important parameter that can be computed as following (Dou, *et al.*
206 1995):

207 $$g_{b,L} = K_0 \frac{\gamma_s U' \overline{U}^3}{\frac{\gamma_s - \gamma}{\gamma} g \omega_L C_0^2} \tag{22}$$

208 where K_0=0.001 ; $C_0 = h^{1/6}/(ng^{1/2})$; $U' = \begin{cases} \overline{U} - U_c, & \overline{U} > U_c \\ 0, & \overline{U} \le U_c \end{cases}$; U_c = the incipient velocity of
209 sediment, which can be calculated by:

210 $$U_c = 0.265 \ln\left(\frac{11h}{\Delta}\right) \sqrt{\frac{\gamma_s - \gamma}{\gamma} gd + 0.19 \frac{\varepsilon_k + gh\delta}{d_{b50}}} \tag{23}$$

211 in which d_{b50} =the medium bedload diameter; $\varepsilon_k = 2.56 \times 10^{-6}\ \mathrm{m^3/s^2}$; $\delta = 0.12 \times 10^{-6}\ \mathrm{m}$; Δ =
212 roughness height of rive bed and can be determined as:

213 $$\Delta = \begin{cases} 0.5\mathrm{mm}, & D_{50} \le 0.5\mathrm{mm}, \\ D_{50}, & D_{50} > 0.5\mathrm{mm}. \end{cases} \tag{24}$$

214

2.6. Recovering saturation coefficient

Recovering saturation coefficient in (6) and (7) can be evaluated by (Wei *et al.* 1997)

$$\alpha_L = \begin{cases} 0.001/\omega_L^{0.3}, & S_L \geq S_L^* \\ 0.001/\omega_L^{0.7}, & S_L < S_L^* \end{cases} \tag{25}$$

3. Numerical methods

3.1. Discretization of the governing equations

The general governing equation (10) is discretized with finite volume method (FVM) (Versteeg and Malalasekera 1995). The computational domain is rectangular in the BFC system and can be easily divided into a series of small rectangles, as shown in Figure 1. Collocated grid system is adopted in this study. In order to avoid the checkerboard pressure difference, momentum interpolation method (Rhie and Chow, 1983) is used. The representative control volume is ΔV and its centre is node *P*. The east, west, south and north faces of the control volume are *e*, *w*, *s* and *n*, respectively. The east, west, south and north neighbor nodes of P are *E*, *W*, *S* and *N*, respectively. Integrating Eq. (10) over the control volume ΔV yields:

$$\begin{aligned} &\int_{\Delta V} \frac{\partial}{\partial t}(h\Phi)dV + \int_{\Delta V} \frac{1}{J}\frac{\partial}{\partial \xi}(hU\Phi)dV + \int_{\Delta V} \frac{1}{J}\frac{\partial}{\partial \eta}(hV\Phi)dV \\ &= \int_{\Delta V} \frac{1}{J}\frac{\partial}{\partial \xi}(\frac{\alpha h\Gamma_\Phi}{J}\frac{\partial \Phi}{\partial \xi})dV + \int_{\Delta V} \frac{1}{J}\frac{\partial}{\partial \eta}(\frac{\gamma h\Gamma_\Phi}{J}\frac{\partial \Phi}{\partial \eta})dV + \int_{\Delta V} S_\Phi(\xi,\eta)dV \end{aligned} \tag{26}$$

The first term (i.e. unsteady term, represented by I_t) on the left hand side is discretized by the first order implicit scheme:

$$I_t \doteq \frac{h_P\Phi_P - h_P^*\Phi_P^*}{\Delta t} J_P \Delta\xi\Delta\eta \tag{27}$$

where $\Delta t, \Delta\xi, \Delta\eta$ are time step, spatial steps in ξ and η directions, respectively. Subscript *

represents the variable of the last time step.

The second and third terms (i.e. convective terms, represented by I_C) on the left hand side are discretized using an improved QUICK scheme developed by Hayase, *et al.* (1992). In this scheme, a deferred correction method presented by Khosla and Rubin (1974) is used to improve the QUICK scheme.

$$I_C = E_e - E_w + E_n - E_s \tag{28}$$

where

$$E_e = [|F_e,0|]\left(\Phi_P + \frac{1}{8}(3\Phi_E - 2\Phi_P - \Phi_W)^*\right) + [|-F_e,0|]\left(\Phi_E + \frac{1}{8}(3\Phi_P - 2\Phi_E - \Phi_{EE})^*\right) \tag{29}$$

$$E_w = [|F_w,0|]\left(\Phi_W + \frac{1}{8}(3\Phi_P - 2\Phi_W - \Phi_{WW})^*\right) + [|-F_w,0|]\left(\Phi_E + \frac{1}{8}(3\Phi_W - 2\Phi_P - \Phi_E)^*\right) \tag{30}$$

$$E_n = [|F_n,0|]\left(\Phi_P + \frac{1}{8}(3\Phi_N - 2\Phi_P - \Phi_S)^*\right) + [|-F_n,0|]\left(\Phi_N + \frac{1}{8}(3\Phi_P - 2\Phi_N - \Phi_{NN})^*\right) \tag{31}$$

$$E_s = [|F_s,0|]\left(\Phi_S + \frac{1}{8}(3\Phi_P - 2\Phi_S - \Phi_{SS})^*\right) + [|-F_s,0|]\left(\Phi_P + \frac{1}{8}(3\Phi_S - 2\Phi_P - \Phi_N)^*\right) \tag{32}$$

In which $[|F_e,0|] = max(F_e,0)$, $F_e = (hU\Delta\eta)_e$, $F_n = (hV\Delta\xi)_n$.

As a result, the scheme has not only the third order accuracy, but is also diagonally dominant and can be easily programmed.

The first and second terms on the right hand side (i.e. diffusion terms, represented by I_D) are discretized using the second order central difference scheme.

$$I_D = D_e(\Phi_E - \Phi_P) - D_w(\Phi_P - \Phi_W) + D_n(\Phi_N - \Phi_P) - D_s(\Phi_P - \Phi_S) \tag{33}$$

where

$$D_e = \left(\frac{\alpha\Gamma_\Phi h}{J}\right)_e \frac{\Delta\eta}{(\delta\xi)_e}, D_n = \left(\frac{\gamma\Gamma_\Phi h}{J}\right)_n \frac{\Delta\xi}{(\delta\eta)_n}.$$

The last term on the right hand side (the source term, represented by I_S) can be dealt with using the following local linear method:

$$I_{S_\Phi} = I_{S_{\Phi C}} + I_{S_{\Phi P}}\Phi_P \tag{34}$$

where $I_{S_{\Phi P}} \le 0$. As for momentum equations, the source terms are as following:

$$I_{S_{uC}} = -\Delta\xi\Delta\eta\left[gh(z_\xi y_\eta - z_\eta y_\xi) + \frac{\partial}{\partial\xi}\left(\frac{\beta\Gamma_u h}{J}\frac{\partial u}{\partial\eta}\right) + \frac{\partial}{\partial\eta}\left(\frac{\beta\Gamma_u h}{J}\frac{\partial u}{\partial\xi}\right) + \frac{1}{J}\frac{u\sqrt{\gamma}}{\sqrt{u^2+v^2}}\frac{\partial}{\partial\eta}\left(|\bar{u}|\bar{u}\phi\right)\right]$$

$$I_{S_{vC}} = -\Delta\xi\Delta\eta\left[gh(-z_\xi x_\eta + z_\eta x_\xi) + \frac{\partial}{\partial\xi}\left(\frac{\beta\Gamma_v h}{J}\frac{\partial v}{\partial\eta}\right) + \frac{\partial}{\partial\eta}\left(\frac{\beta\Gamma_v h}{J}\frac{\partial v}{\partial\xi}\right) + \frac{1}{J}\frac{v\sqrt{\gamma}}{\sqrt{u^2+v^2}}\frac{\partial}{\partial\eta}\left(|\bar{u}|\bar{u}\phi\right)\right]$$

$$I_{S_{uP}} = I_{S_{vP}} = -\frac{gn^2\sqrt{u^2+v^2}}{h^{1/3}} J_P\Delta\xi\Delta\eta.$$

The discretized equation of the general governing equation (10) using the above discretized scheme is as following:

$$a_P\Phi_P = a_E\Phi_E + a_W\Phi_W + a_N\Phi_N + a_S\Phi_S + I_{S_{\Phi C}} + S^*_{ad} \tag{35}$$

where

$$a_E = D_e + [|-F_e, 0|], a_W = D_w + [|F_w, 0|] \ , \ a_N = D_n + [|-F_n, 0|], a_S = D_s + [|F_s, 0|],$$

$$a_P = a_E + a_W + a_N + a_S + F_e - F_w + F_n - F_s + a^*_P - I_{S_{\Phi P}}, b = a^*_P\Phi^*_P + I_{S_{\Phi C}} \ ,$$

$$a^*_P = \frac{h^*_P}{\Delta t} J_P\Delta\xi\Delta\eta, \ S^*_{ad} = (S^*_{ad})_e + (S^*_{ad})_w + (S^*_{ad})_n + (S^*_{ad})_s,$$

$$(S^*_{ad})_e = \frac{1}{8}(3\Phi_E - 2\Phi_P - \Phi_W)^*[|F_e, 0|] + \frac{1}{8}(3\Phi_P - 2\Phi_E - \Phi_{EE})^*[|-F_e, 0|],$$

$$(S^*_{ad})_w = \frac{1}{8}(3\Phi_P - 2\Phi_W - \Phi_{WW})^*[|F_w, 0|] + \frac{1}{8}(3\Phi_W - 2\Phi_P - \Phi_E)^*[|-F_w, 0|],$$

$$(S_{ad}^{*})_n = \frac{1}{8}(3\Phi_N - 2\Phi_P - \Phi_S)^{*}[|F_n, 0|] + \frac{1}{8}(3\Phi_P - 2\Phi_N - \Phi_{NN})^{*}[|-F_n, 0|],$$

$$(S_{ad}^{*})_s = \frac{1}{8}(3\Phi_P - 2\Phi_S - \Phi_{SS})^{*}[|F_s, 0|] + \frac{1}{8}(3\Phi_S - 2\Phi_P - \Phi_N)^{*}[|-F_s, 0|].$$

Collocated grids SIMPLEC algorithm in body fitted coordinate system (Van Doormaal and Raithby 1984) is used to solve the coupled problem of water level and velocities. The discretized equations are five-diagonal, which can be solved using alternative direction tridiagonal matrix algorithm (TDMA) (Versteeg and Malalasekera 1995).

3.2. Semi-coupled scheme for sediment model

In this study, a semi-coupled scheme is developed by combining the advantages of coupled and decoupled schemes. In the process of long time simulation of sediment transport when river bed changes slowly, the bed elevation change each time step has minimal impacts on flow field, therefore, it is unnecessary to update the hydraulic elements each time step. Thus, in order to reduce the computational cost, the hydraulic module runs intermittently while the sediment module keeps running all the time. In the semi-coupled scheme, after the sediment module starts to run, the hydraulic module will stop running for a certain number of time steps (for example, 1000-5000 time steps), then it will run again. After running for certain time steps (such as 60-120 time steps) to update the hydraulic elements, it will then stop running. The process is repeated until the required accuracy is reached.

Let *t* be simulating time, *t0_flow* the initial simulation time for the flow module, *t1_flow* the flow module working time each time, *t2_flow* the time interval between two adjacent times when flow

297 module is started, *t_max* the whole simulation time. The procedure of this semi-coupled scheme is
298 detailed as following:
299
300 ***Algorithm of semi-coupled scheme:***
301 Step 1. If $t \leq t0\_flow$, only the flow module is running；
302 Step 2. If $t0\_flow < t < t\_max$, the sediment module is running.
303 Step 3. If $t0\_flow < t < t\_max$, and mod (t, $t2\_flow$)$<t1\_flow$, the flow and sediment modules are
304 running together；otherwise, only the sediment module is running.
305 Step 4. If $t > t\_max$, stop.
306 where *mod* is a function which means modulus and *mod* (t, $t2\_flow$) is the remainder when t is
307 divided by $t2\_flow$. In this study, time step dt=12s, $t0\_flow$=5h, $t1\_flow$=1h, $t2\_flow$=12h.
308 Numerical experiments indicate that the computational time of the semi-coupled scheme is about
309 60% of the coupled scheme.
310
311 ***3.3. Boundary and initial conditions***
312 We choose two adjacent field measurements to verify the sediment model. The field measurements
313 were conducted on December 6, 2008 and on July 17, 2009, respectively. The time interval
314 between the two measurements is 203 days. Water discharge and sediment concentration are given
315 at the inlet based on values interpolated by field data measured on December 6, 2008 and on July
316 17, 2009. The turbulence kinetic energy (k) and its dissipation rate (ε) at the inlet are calculated
317 using empirical formulae (Rodi 1993). On the water outlet boundary, water level is specified based
318 on the values by interpolating the field data measured on December 6, 2008 and on July 17, 2009.

Other variables are dealt with using the fully developed condition. On the wall boundary, no-slip boundary condition is applied. The velocity parallel to the river bank at the first cell is estimated using standard wall function (Guo, et al. 2008).

In order to study the flow and sediment transport in the studied reach, four cases are used based on discharge and sediment concentration at the inlet. The boundary conditions of the four cases are presented in Table 1. Case 1 is set according to the field measured data on December 6, 2008, while Case 2 is set according to the data measured on July 17, 2009. Case 3 and Case 4 are set according to the hydrological data in the past years. Cases 1 and 4 represents the hydraulic conditions of dry and flood seasons, respectively, while Cases 2 and 3 represents hydraulic condition of wet season.

The initial values are based on field measured data on December 6, 2008, including the position of cross-sections, water level, maximum water depth, average water depth, river width, average velocity of 14 cross-sections (see Table 2). The initial water level at each grid is set as the same as the water level at the outlet. u, v and S_L at each grid are set as zero, except for the grids at the inlet. However, k and ε can not be set as zero, otherwise, the simulation process will stop unexpected or be unstable. In the simulations, the initial values of k and ε are set as 0.1 m^2/s^2 and 0.0001 m^2/s^2, respectively, based on the authors' experience.

The suspended and bedload sediment at the inlet section is divided into three groups with the medium diameter being 0.0249 mm and 10 mm, respectively. The representative diameters and

related percentage for both the suspended and bedload sediment are listed in Table 3. The bed material is divided into six groups, whose representative diameters and their percent content are also presented in Table 3. The initial percentage contents of the suspended and bedload are set as the same as the values at the inlet. Some representative diameters of the initial bed material of the whole reach are: d_{50} =10 mm, d_m =15.5 mm, $d_{25} = 1$ mm, $d_{35} = 4$ mm, $d_{75} = 20$ mm, $d_{90} = 70$ mm and $d_{95} = 100$ mm, where d_m = the mean diameter, d_a = the sediment diameter that a% is less than that in the size gradation curve (a=25, 35,50,75,90,95).

3.4. Mesh generation

In the computational domain, along longitudinal direction (ξ-direction), 131 grids are assigned, while along transverse direction (η-direction), 31 grids are set. Poisson equation method is used to make body-fitted coordinate transformation and grid generation (Versteeg and Malalasekera 1995). The total number of grids and cells are 4991 and 4800, respectively. To better fit the complex boundary, non-uniform meshes with arbitrarily spatially dependent size were used. This allows for locally refining the concerned regions (e.g. near bends) with small meshes and has the advantage of flexibly assigning meshes in the computational domain. Along transverse direction, there are 30 cells, in which 5 non-uniform cells near left bank and near right bank, respectively. The gird length of the 5 cells near bank increases from bank to interior. Figure 2 shows the mesh distribution near banks and bends.

4. Results and discussions

4.1. Description of the computational domain and numerical simulation

The Shapotou Reservoir in the Yellow River is located in Ningxia Hui Autonomous Region in China. The studied reach is about 13.4km long, as shown in Figure 3. Twenty cross-sections (e.g. SH1-SH15, SHJ1-SHJ5) are assigned in the studied reach, in which SH15 is the inlet, and SH1 is the outlet. The studied reach consists of five bends: Bend A (from SH15 to SH13), Bend B (from SH13 to SH11), Bend C (from SH11 to SH7), Bend D (from SH7 to SH2) and Bend E (from SH2 to SH1). Bends A and B are near the exit of the Heishan Gorge, where the river is deep and narrow, and the current is rapid. The averaged water width at bend A and Bend B is about 135m with the normal water level gradient being about 0.03%. Bends C, D and E are near the Shapotou Dam, where the river is wide and shallow (the averaged water width is about 300 m), and the current is slow. The normal water level gradient is about 0.006% .

In the simulation, the semi-coupled scheme in the 2D depth averaged RNG k-ε sediment model is applied. The software of Matlab 7.1 is used to program, and the numerical simulation is performed on an IBM work station. The CPU of the work station is two cores Intel ® Xeon 2.0G Hz; the memory is 4.0GB; the operation system is Ghost-Server2003 SP2. Typical numerical simulation takes about 16 days.

4.2. Sediment setting velocity

The sediment setting velocities of the six representative groups in the studied reach are calculated by (20) and modified by (21), as listed in Table 4.

The sediment setting velocity is affected by the sediment concentration. Here we assume that the sediment concentration is S=10kg/m^3 and the sediment concentration by volume is $S_v=S/\rho_s$=0.0038 (ρ_s = density of sediment=2650kg/m^3). It is seen that the same sediment concentration has different influence for the setting velocity of various grain size groups. The correction rate is bigger for fine sediment than that for coarse sediment. In other words, sediment concentration has larger effect on fine sediment than on the coarse one.

4.3. Suspended sediment carrying capacity

The suspended sediment carrying capacity is calculated using (17) and (18) for different group sediment carrying capacity. Because the numerical results about suspended sediment carrying capacity of the four cases are similar, only the result under the condition of Case 2 is presented in this paper. Figure 4 shows the distribution of sediment concentration, total and group suspended sediment carrying capacities along the centerline of the studied river reach. As shown in Figure 4, both total and group sediment carrying capacities decrease along the way. It can also be found that the carrying capacity of the second sediment group is the largest among the three sediment groups, while the carrying capacity of the third sediment group is the smallest, which is consistent with the sediment concentration of the three groups at the inlet.

4.4. Bedload sediment transport rate

In this study, four different methods are applied to calculate bedload sediment transport. The first method (Method I) is to calculate group bedload transport rate by (22), then summing them to obtain the total transport rate. The second method (Method II) is to calculate ω by (20) and (21),

where the representative sediment diameter (d) is chosen as d_{35}; then replacing ω_L with ω in (21) to calculate the total bedload sediment transport rate. The third method (Method III) is the same as Method II, except that the representative sediment diameter is d_m. The fourth method (Method IV) is the same as Method II, except that d_{50} is chosen as the representative sediment diameter.

From Table 5, it can be seen that the bedload transport rates calculated using the four methods are different. Generally speaking, for non-uniform bedload sediment, it would be more accurate to divide bedload sediment into several groups when computing its transport rate. Therefore, the result calculated using Method I is the most reliable. The result calculated by Method II is closer to the result of Method I, indicating that the transport rate of non-uniform bedload sediments can be calculated using the formula for computing the transport rate of uniform bedload sediments when the representative sediment diameter is chosen as d_{35} for the flow and sediment conditions investigated here. This result is consistent with the conclusion of Einstein (Zhang, 1988).

4.5. Comparison between measured and calculated velocities

Figure 5 shows the comparison of the simulated and field measured (on July 16 2009) depth averaged velocities on three selected cross-sections, i.e. SH7, SH5, SHJ2, which are near the inlet, apex, and outlet of Bend D, respectively. Figure 5(1) also shows the comparison of the depth averaged velocities calculated using two methods: Simulation 1 and Simulation 2. In Simulation 1, the circulation flow is not taken into account, while this has been taken into account in Simulation 2. It is seen that the simulated velocity using the second approach is better compared to the

measured data than that using the first method, indicating that the modified plane 2D RNG *k-ε* model is capable of simulating the effect of the circulation flow in natural rivers. In general, good agreements between simulated and field measured velocities at three cross sections are obtained.

4.6. Comparison between measured and calculated river bed deformation

Figure 6 is the plot of the simulated and field measured (on July 17 2009) bed elevation along the longitudinal direction. It is seen that the simulated bed elevation is in good agreement with the measured data. From SH11 to SH9, the river bed is scoured, while from SHJ5 to SH2, the river bed is deposited. The deposit thickness varies significantly from SH2 to SH5 with the largest deposition taking place in SH2 (where the average deposit thickness is over 1 m), while little deposit takes place at SH5 (where the average deposit thickness is only about 0.01 m).

In Figure 7, the measured and the simulated bed elevations at three typical cross sections are plotted. The three cross sections are SH10, SHJ5 and SH7, which are near the inlet, the bend apex, and the outlet of Bend C, respectively. It is seen from Figure 7 that the simulated bed elevation agrees well with the measured data on these cross sections, indicating that the 2D depth averaged RNG k-ε sediment model can reasonably simulate the bed deformation in the studied reach. The bed on SH10 is scoured as a whole except some small areas near the river banks. The bed near the left bank of SHJ5 and SH7 is deposited and the bed near the right bank of the two cross-sections is scoured. Because the left bank is the convex bank , while the right bank is the concave bank in Bend C, the above phenomenon is in consistence with the general rule of sediment transport in a bend.

4.7. Suspended sediment transport

Figure 8 shows the distribution of suspended sediment concentration along the centerline of the studied reach under the condition of Case 2 with the sediment concentration at the inlet being set as 0.51, 3.53, 10 and 20 kg/m^3, respectively. From Figure 8, it is seen that the suspended sediment concentration in the studied reach increases with increasing the suspended sediment concentration at the inlet. As the river of the studied reach becomes wider and shallower as the flow moves downstream, the flow becomes slower and the sediment carrying capacity becomes weaker accordingly along the way, leading to the decrease of the suspended sediment concentration along the way.

4.8. The effect of discharge on river bed deformation

In order to investigate the effect of the discharge at the inlet on the bed deformation, numerical simulations were conducted for four cases. The conditions of the four cases are shown in Table 1 except that the sediment concentration at the inlet is set as 3.53kg/m^3. Figure 9 shows the simulated bed elevation after 10 days development for all four cases. The bed is deposited near the inlet for Cases 1 and 2, while the bed is scoured near the inlet under the condition of Cases 3 and 4. The reason is that the average velocities for the Cases 1 and 2 are small, and the suspended sediment capacities are smaller than the sediment concentration. As a result, the bed is deposited near the inlet. However, after flow moves a certain distance, a balance between deposition and scour is reached. The position of balance is about 9.5km from the inlet for Case 1, and it is near SH5; while for Case 2, it is about 10.5km from the inlet and near SH4. The discharges and average

velocities of the Cases 3 and 4 are larger, and the suspended sediment capacities of the two cases are larger than sediment concentration. Therefore, the bed is scoured near the inlet. Similar to Cases 1 and 2, a balance between deposition and scour is reached after the flow moves a certain distance away from the inlet. For Case 3, the position is about 4.5km from the inlet and near SH10; while for Case 4, the position is about 6km from the inlet and near SHJ5. From above analysis, it can be concluded that the discharge at the inlet has significant influence on the bed deformation near the inlet. However, after the flow moves a certain distance, the influence becomes weaker and weaker.

4.9. River bed deformation caused by bedload sediment

Though the bed deformation is mainly caused by the suspended sediment transport, the bedload sediment transport can also have significant effect on the bed deformation for some certain situations. To investigate the effect of bedload sediment transport on the river bed deformation, the numerical simulation is conducted for four cases with the same suspended sediment concentration at the inlet being 3.53kg/m^3. Figure 10 shows the percentage of the absolute thickness deposited or scoured by suspended and bedload sediments for four typical cases after 10 days development, respectively. It can be seen that the thicknesses deposited or scoured due to the suspended or bedload sediment transport is quite different. In Cases 1 and 2, the percentage of bed deformation caused by bedload sediment is less than 1%, which is negligible. In Case 3, the percentage is less than 3% and is still very small and can be neglected. In Case 4, however, the percentage is about 10%, which can not be neglected. Therefore, it can be concluded that the bed deformation caused by bedload sediment can be neglected when the discharge at the inlet is small (less than 1500m^3/s

495 in this study). When the discharge at the inlet is larger (more than 2000m^3/s in this study),
496 however, the bed deformation caused by bedload sediment reaches a certain level and has to be
497 taken into account. .
498
499 ***4.10. The variation of effective bed material granularity***
500 Bed material becomes finer or coarser when the bed is deposited or scoured and it is worth of
501 investigating. Because the simulated results for four cases are similar, only the numerical result of
502 Case 4 is presented and discussed in this paper. Under the condition of Case 4, numerical
503 simulations were conducted for the sediment concentration at the inlet (S_{in}) being 0.51kg/m^3 and
504 10kg/m^3, respectively.
505
506 Figure 11 shows the variation of effective bed material granularity along the river flow direction
507 after 20 days. In Figure 11, the axis x is the distance from the inlet, and the axis y is the percentage
508 of each group effective bed materials. The percentage of the initial bed material for the six groups
509 is 0.2%, 3.8%, 17.9%, 12.7%, 36.5%, 28.9%, respectively, as shown by the dash line in Figure 11.
510
511 When S_{in} = 0.51kg/m^3, the river bed is scoured as a whole and the bed material size gradation is
512 changed after 20 days' scouring. In Figure 11(a), it is seen that the percentage of the first three
513 groups (Groups 1-3) of bed material decreased compared with the initial value, especially for
514 Groups 2 and 3. The decreasing tendency becomes weaker with the distance and reaches the
515 minimum at the distance of 8.5km from the inlet (near SH6). Meanwhile, the percentage of the last
516 three groups (Groups 4-6) of bed material increased compared with the initial value. The

increasing tendency also becomes weaker with the distance and reaches the minimum near SH6. And after SH6, the bed material granularity is almost not changed for all of the 6 groups. This means that bed becomes coarser when the bed is scouring. However, after SH6, the sediment concentration at the inlet has little influence to the bed deformation and variation of bed material granularity, as shown by Figure 9 and Figure 11.

When S_{in}=10kg/m^3, the situation is different and complicated. As shown in Figure 11(b), the bed material percentage of Groups 1-3 increases, while the percentage of Groups 4-6 decrease as a whole compared with the initial value. In Figure 11(b), it can also be found that the percentage of the first three groups of the bed material increases with the distance and reaches the maximum near SH6. The percentage of these groups then decreases with the distance. To the contrary, the last three groups of the bed material decreases with the distance and reaches the minimum near SH6 and increases again to the outlet. This means that the river bed becomes finer compared with the initial value when it is deposited. Similar to the condition when S_{in}=0.51 kg/m^3, after SH6, the sediment concentration at the inlet has little influence to the bed deformation and variation of bed material granularity.

5. Conclusions

In this study, a 2D depth averaged RNG k-ε sediment model including the effects of secondary currents is developed, which considers the effects of the non-uniform suspended and bedload sediment transport on the bed deformation. In the model, the variation of effective bed material granularity is included. A semi-coupled scheme is developed by combining the coupled and

539 decoupled schemes to improve the accuracy of the numerical simulation (compared with the
540 decoupled scheme) and save computational time (compared with the coupled scheme). Numerical
541 simulations have been performed for four typical cases to investigate the sediment transport and
542 bed deformation in the upper reach of the Yellow River. Comparison between the numerical
543 results and field measurements indicates that the 2D depth averaged RNG k-ε sediment model can
544 reasonably simulate the sediment transport and the resultant bed deformation of rivers with
545 continuous bends. River bed deformation induced by suspended and bedload sediment transports
546 has been investigated. It is found that the bed deformation caused by bedload sediment transport
547 can be neglected when the discharge at the inlet is small (less than 1500m^3/s in this study). The
548 results also show that the discharge at the inlet has significant effect on the bed deformation near
549 the inlet. The influence, however, becomes weaker as the flow moves downstream.
550
551 The variation of effective bed material granularity has been examined. It is concluded that the bed
552 material granularity becomes finer when the bed is deposited. When the bed is scoured, the bed
553 material granularity becomes coarser. The bed material granularity becomes finer along the way in
554 the studied reach no matter it is deposited or scoured. The sediment concentration at the inlet has
555 significant influence for bed material granularity near the inlet. However, the influence becomes
556 weaker with the distance from the inlet.
557
558 **6. Acknowledgements**
559 The authors acknowledge with thanks the following institutes for assisting this study: Ningmeng
560 Hydrographic & Water Resource Office of Yellow River Water Conservancy Committee of China,

and Ningxia Shapotou Hydraulic Power Plant of China. Constructive comments and suggestions from the Editor and Reviewers have greatly improved the quality of the paper.

7. References

Dou, G.R., Dong, F.W., Dou, X.P., Li, T.L., 1995. Mathematical modeling of sediment transport in estuaries and coastal regions. *Science in China(Series A)*, 38 (10):1251-1260.

Duan, J.G., Nanda, S.K., 2006. Two-dimensional depth-averaged model simulation of suspended sediment concentration distribution in a groyne field. *Journal of Hydrology*, 327, 426-437.

Duan, J.G., Julien, P.Y., 2010. Numerical simulation of meandering evolution. *Journal of Hydrology*, 391: 34-46.

Falconer, R.A. 1992. Flow and water quality modelling in coastal and inland water. *J. Hydraul. Res.*, 30, 437-452.

Guo, Y.K., Wang, P.Y., Zhou, H., 2007. Numerical modelling of the flow past irregularities in a pressure conduit, *ASCE J. Hydr. Eng.*, 133(6): 698-702.

Guo, Y.K., Zhang, L.X., Shen, Y.M., Zhang, J.S., 2008. Modeling study of free overfall in a rectangular channel with strip roughness, *ASCE J. Hydr. Eng.*, 134(5): 664–667.

Guo, Y.K., Wu, X.G., Pan, C.H., Zhang, J., 2012. Numerical Simulation of the Tidal Flow and Suspended Sediment Transport in the Qiantang Estuary, *ASCE Journal of Waterway, Port, Coastal and Ocean Engineering*, 138: 192-203.

Hayase, T., Humphrey, J.A.C., Greif, G.., 1992. A consistently formulated QUICK scheme for fast and stable convergence using finite volume iterative calculation proceeding. *J. Comput. Phys.*, 98:108-118.

583 Hung, M.C., Hsieh, T,Y,, Wu, C.H., Yang, J.C., 2009. Two-Dimensional nonequilibrium
584 noncohesive and cohesive sediment transport model. *J. Hydr. Eng.(ASCE),* 135(5) : 369-382
585 Jing, H.F., Guo, Y.K., Li, C.G., Zhang, J.S., 2009. Three-dimensional numerical simulation of
586 compound meandering open channel flow by the Reynolds stress model. *Int. J. Numer. Mech.*
587 *Fluids*, 59, 927-943.
588 Jing, H.F., Li, C.G., Guo, Y.K., Xu, W.L., 2011. Numerical simulation of turbulent flows in
589 trapezoidal meandering compound open channels. *Int. J. Numer. Mech. Fluids*, 65, 1071-1083.
590 Khosla, P.K., Rubin, S.G., 1974. A diagonally dominant second order accurate implicit scheme.
591 *Computer & Fluids*, 2:207-209.
592 Li, S.S., Millar, R.G., 2011. A two-dimensional morphodynamic model of gravel-bed river with
593 floodplain vegetation. *Earth Surface Process & Landforms*, 36(2): 190-202.
594 Lien, H.C., Hsieh, T.Y., Yang, J.C., Yeh, K.C., 1999. Bend-flow simulation using 2D
595 depth-averaged model. *ASCE J. Hydr. Eng.*, 125, 1097-1108.
596 Nagata, N., Hosoda, T., Muramoto, Y., 2000. Numerical analysis of river channel processes with
597 bank erosion. *ASCE J. Hydr. Eng.*, 126 (4): 243 -252.
598 Rhie, C.M., Chow, W.L., 1983. A numerical study of the turbulent flow past an isolated airfoil
599 with trailing edge separation. *AAIA J.*, 21:1525-1532.
600 Rodi, W., 1993. *Turbulence models and their application in hydraulics: A state-of-the-art review,*
601 *3rd Ed.*, Balkema, Rotterdam, the Netherlands.
602 Serrano-Pacheco, A., Murillo, J., Garcia-Navarro, P., 2012. Finite volumes for 2D shallow-water
603 flow with bed-load transport on unstructured grids, *Journal of Hydraulic Research*, 50(2):
604 154-163.

605 Van Doormaal, J.P., Raithby, G.D., 1984. Enhancement of SIMPLE method for predicting
606 incompressible fluid flows. *Numer. Heat Transfer*, 7(2): 147-163.
607 Versteeg, H.K., Malalasekera, W., 1995. *An introduction to computational fluid dynamics*.
608 Addison Wesley Longman Limited, England.
609 Wei, Z.L., Zhao, L.K., Fu, X.P., 1997. Research on mathematical model for sediment in Yellow
610 River, *J. Wuhan University of Hydro. & Electric Eng*., 30(5):21-25.
611 Yakhot, V., Orzag, S.A., 1986. Renomalization group analysis of turbulence: basic theory. *J.*
612 *Scient Comput.*, 1, 3-11.
613 Zhang, H.W., Zhang, Q., 1992. Formula of Sediment Carrying Capacity of the Yellow River .
614 *Yellow River*, (11):6-9.
615 Zhang, R.J., 1988. *River Sediment Dynamics(the second edition)*. Beijing: Water Conserversy and
616 Hydropower of China.
617

Modelling of sediment transport and bed deformation in rivers with continuous bends*

Hefang Jing[a†] *Chunguang Li*[a] *Yakun Guo*[b] *Lixiang Zhang*[c] *Lijun Zhu*[d] *Yitian Li*[e]

[a] Res. Inst. Numer. Comput. Eng. Appl., Beifang University of Nationalities, Yinchuan 750021, China.
[b] School of Engineering, University of Aberdeen, Aberdeen, AB24 3UE, UK.
[c] Department of Engineering Mechanics, Kunming University of Science and Technology, Kunming, 650051, China.
[d] School of Information and Computing Science, Beifang University of Nationalities, Yinchuan 750021, China.
[e] State Key Laboratory of Water Resources and Hydropower Engineering Sciences, Wuhan University, Wuhan 430072, China.

Formatted: Footnote Text, Justified, Line spacing: single

Abstract

A two dimensional (2D) RNG *k-ε* sediment model ~~integrating~~ including the effects of secondary currents is developed to simulate the sediment transport and bed deformation in rivers with continuous bends. ~~The~~ Nn~~o~~on-uniform suspended and bedload sediment transports and the variation of effective bed material size distribution are included in the model. A semi-coupled ~~algorithm~~ scheme ~~about the flow and sediment modules in the~~ for sediment model is ~~designed~~proposed, which can be used for simulating both the long- and short term sediment transport whenever riverbed changes. The model is applied to simulate the flow and sediment transport in the upper reach of the Yellow River which is a typical natural river reach with continuous bends. ~~A series of numerical simulations are conducted for Shapotou reservoir in the upper reach of the Yellow River for four typical cases.~~ The river bed deformations caused by suspended and bedload sediments are investigated. Good agreement between the numerically simulated results and the field measurements is obtained, indicating that the model is capable of ~~can~~ simulate~~e~~ing the sediment transport and predicting the bed deformation of rivers having

* **Grant sponsor:** the Major Research Plan Project, National Natural Science Foundation of China (grant number: 91230111); Project of Science and Technology of Colleges in Ningxia, China (grant number: NGY2012097); Project of Beifang University of Nationalities, China (grant number: 2012XZK05); Foreign Expert Project of Beifang University of Nationalites, China.

† Address for Correspondence: Dr. Hefang Jing, Res. Inst. Numer. Comput. Eng. Appl., Beifang University of Nationalities, Yinchuan 750021, China. Email: jinghef@163.com. Tel: +86 951 2068011

continuous bends with reasonable accuracy.

Key words :RNG k-ε turbulence model, bed deformation ,suspended sediment, bedload sediment, bed material ~~composition~~granularity.

NOMENCLATURE

C	Chezy coefficient	h	water depth
D_{50}	medium diameter of bed material	k	turbulent kinetic energy
P_{mL}	bed material granularity	n	Manning coefficient
$P_{mL,0}$	original bed material granularity	u	velocity in x direction
S	sediment concentration	v	velocity in y direction
S_L	group sediment concentration	z	water level
S_v	sediment concentration by volume	α_L	group saturation recovery coefficient of sediment
S^*	sediment carrying capacity	γ	water specific gravity
S_L^*	group sediment carrying capacity	γ'	dry specific gravity of sediment
$\overline{U}$	depth averaged velocity	κ	Karman constant
Z	bed elevation	ε	turbulence dissipation rate
$Z_{S,L}$	the deposition thickness of the L-th group suspended sediment	ν	water viscosity
$Z_{b,L}$	the deposition thickness of the L-th group bedload	ν_t	water eddy viscosity
d_{50}	medium diameter of suspended sediment	γ_s	sediment specific gravity
d_m	averaged diameter of suspended sediment	γ_m	Specific gravity of muddy water
d	diameter of sediment	ω	sediment settling velocity
g	gravity acceleration	ω_L	sediment settling velocity of the L-th group sediment

Formatted Table

1. Introduction

~~The~~ Fflow and sediment transport near hydraulic structures in rivers have been extensively studied using various approaches, such as theoretical analysis, laboratory experiments and numerical simulation. Among these approaches, ~~the~~ numerical simulation has advantages in several aspects and has been increasingly used (Falconer 1991; Guo *et al.* 2007). ~~The mathematical models in the numerical simulation can be divided into three different groups according to their space dimensionality: one dimension (1D), two dimension (2D) and three dimension (3D). Because 1D sediment models are simpler and less time consuming, in the past decades, many 1D sediment models such as HEC-6 model (Feldman 1981) , MIKE11 model (Rahman, et al. 2011), have been developed and widely used. However, these 1D models can only simulate stream-wise hydraulics and sediment elements, and can not reflect the elements along transverse or vertical directions. As a result, 1D sediment models usually are less reliable when they are used in curved rivers or rivers with their width changing sharply. In this situation, 3D sediment models, which can simulate the hydraulics and sediment elements in stream-wise, transverse and vertical directions, should be applied. Chen (1986) conducted 3D numerical simulation of sediment transport in an estuary. Ruther and Olsen (2005) simulated the sediment transport in a narrow and deep bends using a 3D sediment model. Bui and Rutschmann (2010) conducted 3D numerical simulation of bed deformation in a laboratory bend.~~

~~Though 3D models can produce accurate simulation for some cases, they are more complex and time consuming. Therefore, it is not practical to apply them for simulating a long reach of rivers.~~

Formatted: Font: Italic

In natural rivers, the horizontal scale is usually much greater than the vertical scale; therefore, it is suitable to apply the depth averaged ~~plane~~ 2D model (Guo et al. 2012). Generally speaking, ~~N~~numerical simulation using these models not only requires less computational time than three dimensional (3D) sediment models(particularly for large scale simulation), but also is more accurate than that of one dimensional (1D) sediment models. As a result, ~~plane~~ depth averaged 2D sediment models are widely applied in engineering to study sediment transport and river bed deformation. Nagata *et al.* (2000) developed a 2D sediment model for inviscid river banks. ~~Papanicolaou et al. (2008) reviewed sediment transport modeling and predicted its future developments.~~ Hung *et al.* (2009) developed an unsteady 2D depth-averaged model for nonuniform sediment transport in alluvial channels, taking ~~into account~~ the transport mechanisms of cohesive and noncohesive sediment, the suspended sediment and bedload into account. Duan ~~et al~~and Julien~~.~~ (2010) conducted 2D numerical simulation for a laboratory bend, considering transport of suspended sediment and bedload, and river bed deformation. Li ~~et al.~~and Millar (2011) developed 2D morphodynamic model of gravel-bed river with floodplain vegetation, considering the effects of riparian and floodplain vegetation on bank strength, floodplain flow resistance, shear stress partitioning, and bedload transport. Serrano-Pacheco *et al.* (2012) conducted two-dimensional bedload transport simulations, in which bedload transport is governed by a power law of flow velocity and by a flow/sediment interaction parameter.

Though ~~T~~these 2D sediment models have been widely used to simulate the sediment transport and bed deformation in river and open channels, many of them are either laminar model, zero equation turbulent model or standard k-ε turbulent model. As such , they cannot be applied to simulate

Formatted: Font: Italic

Formatted: Font: Italic

Formatted: Font: Italic

complicated turbulent flow and sediment transport in rivers with continuous bends in which the effect of secondary currents induced by the bends or curved channels is important.~~but they may not be suitable in simulating some flow patterns and need to be improved. For examples, these 2D sediment models usually cannot simulate the effect of secondary currents in curved channels~~. Some models were modified and taken the effect of secondary currents into account, but they can only be applied to simulate the regular bends in laboratory ~~regular~~ open channels ~~with bends~~, and ~~can not be used~~are difficult to be applied to simulate flow and sediment transport in natural rivers with continuous bends. ~~Many 2D sediment models are laminar model, zero equation turbulent model or standard k-ε turbulent model, which can not be applied to simulate complicated turbulent flow and sediment transport in rivers with continuous bends.~~ Therefore, these 2D sediment models need to be improved before they can be applied to simulate the natural rivers with continuous curves.

The RNG *k*-*ε* model, developed from standard *k*-*ε* model (Versteeg and Malalasekera,1995), has the advantages over the standard *k*-*ε* model. For example, it is more accurate by adding an extra term in the *ε*-equation; can be used to simulate the turbulent eddy with high accuracy and is applicable to simulate the flows of both the high and low Reynolds number (Jing et al. 2009, 2011).

In this study, a plane 2D RNG k-ε sediment model is developed to simulate the flow and sediment transport in the Shapotou reservoir at the upper reach of the Yellow River with continuous bends. The effect of the secondary current on flow and sediment transport is taken into account in the turbulent model. Both ~~T~~the non-uniform ~~transport of both the~~ suspended and

Formatted: Indent: First line: 0.5 ch

non-uniform bedload sediment transports ~~s~~ is included in the model. In addition, the variation of size distribution of effective bed materials is also simulated ~~included~~ in the model. ~~A semi-coupled algorithm is developed by combining the advantages of the coupled and separate algorithms. The~~ ~~d~~Depth averaged velocity, ~~the~~ water level, ~~the~~ transport of suspended sediment and the bed deformation caused by suspended and bedload sediment transports are investigated.

The governing equations of sediment models can be divided into two modules: flow module and sediment module. The first module includes flow continuous equation, momentum equations and turbulence equations, while the second module includes transportation equations of suspended sediment and bedload and bed deformation equations. Therefore, there are two basic schemes to numerically solve sediment models, i.e. coupled scheme and decoupled scheme. In the coupled scheme, the flow and sediment modules are solved simultaneously, while in the decoupled scheme, the flow module is solved first, then the sediment module. In other words, in the decoupled scheme, the flow module will no longer be run after the sediment module starts. Generally speaking, the coupled scheme is suitable for short time numerical simulation with the rapid change of the river bed. It is usually not suitable for long time numerical simulation of sediment transport due to the large CPU time consuming. On the other hand, the decoupled scheme is suitable for long time numerical simulation with the slow variation of river bed as it requires less computing time. Usually, the hydraulic elements, such as water level and velocity, change very slightly in the long time numerical simulation of sediment transport when river bed changes slowly. In this situation, it is not necessary to calculate the flow module every time step from the point of view of computing cost. However, after a certain time steps of running the sediment module, the river bed

deformation accumulates to a degree that can significantly affect the flow elements. In this situation, the flow module needs to be run to account the effect of sediment transport and bed deformation on the flow field. However, in the decoupled scheme, the flow module is stopped forever after sediment module begins to run. Therefore, the decoupled scheme is unreasonable and needs to be improved in order to simulate the effect of the sediment transport on the flow field. This is one of the motivations of this work in which a semi-coupled scheme is developed by combining the advantages of coupled and decoupled schemes. In the proposed scheme, the sediment module keeps running, while the flow module runs intermittently. Therefore, the scheme is efficient and is less time consuming than the coupled scheme and is more accurate than the decoupled scheme. The semi-coupled scheme is not only suitable for simulating both the long and short time sediment transport, but is also capable of treating both the rapid and slow change of the river bed.

2. Mathematical model

2.1. The ~~Plane~~ 2D depth averaged ~~D~~ RNG k-ε model in Cartesian coordinate

The ~~plane~~ 2D depth averaged RNG k-ε sediment model includes two basic modules: hydraulic module and sediment module. The hydraulic module consists of the following equations (Versteeg and Malalasekera~~, et al~~ and Malalsekera~~.~~, 1995; Duan~~, et al.~~ and Nanda 2006; Serrano-Pacheco, *et al*. 2012):

Formatted: Font: Italic

$$\frac{\partial z}{\partial t}+\frac{\partial (hu)}{\partial x}+\frac{\partial (hv)}{\partial y}=0 \tag{1}$$

$$\frac{\partial (hu)}{\partial t}+\frac{\partial (huu)}{\partial x}+\frac{\partial (huv)}{\partial y}=\frac{\partial }{\partial x}\left(\nu_e h\frac{\partial u}{\partial x}\right)+\frac{\partial }{\partial y}\left(\nu_e h\frac{\partial u}{\partial y}\right)-gh\frac{\partial z}{\partial x}-\frac{gn^2u\sqrt{u^2+v^2}}{h^{1/3}} \tag{2}$$

$$\frac{\partial(hv)}{\partial t}+\frac{\partial(hvu)}{\partial x}+\frac{\partial(hvv)}{\partial y}=\frac{\partial}{\partial x}\left(\nu_e h\frac{\partial v}{\partial x}\right)+\frac{\partial}{\partial y}\left(\nu_e h\frac{\partial v}{y}\right)-gh\frac{\partial z}{\partial y}-\frac{gn^2v\sqrt{u^2+v^2}}{h^{1/3}} \quad (3)$$

$$\frac{\partial(hk)}{\partial t}+\frac{\partial(huk)}{\partial x}+\frac{\partial(hvk)}{\partial y}=\frac{\partial}{\partial x}\left(\alpha_k\nu_e h\frac{\partial k}{\partial x}\right)+\frac{\partial}{\partial y}\left(\alpha_k\nu_e h\frac{\partial k}{\partial y}\right)+h(P_k+P_{kv}-\varepsilon) \quad (4)$$

$$\frac{\partial(h\varepsilon)}{\partial t}+\frac{\partial(hu\varepsilon)}{\partial x}+\frac{\partial(hv\varepsilon)}{\partial y}=\frac{\partial}{\partial x}\left(\alpha_\varepsilon\nu_e h\frac{\partial \varepsilon}{\partial x}\right)+\frac{\partial}{\partial y}\left(\alpha_\varepsilon\nu_e h\frac{\partial \varepsilon}{\partial y}\right)+h\left[\frac{\varepsilon}{k}(C_{1\varepsilon}^{*}P_k-C_{2\varepsilon}\varepsilon)+P_{\varepsilon v}\right] \quad (5)$$

And the sediment module includes following equations:

$$\frac{\partial hS_L}{\partial t}+\frac{\partial huS_L}{\partial x}+\frac{\partial hvS_L}{\partial y}=\frac{\partial}{\partial x}\left(\nu_e h\frac{\partial S_L}{\partial x}\right)+\frac{\partial}{\partial y}\left(\nu_e h\frac{\partial S_L}{\partial y}\right)-\alpha_L\omega_L(S_L-S_L^{*}) \quad (6)$$

$$\gamma_s'\frac{\partial Z_{S,L}}{\partial t}=\alpha_L\omega_L(S_L-S_L^{*}) \quad (7)$$

$$\gamma'_s\frac{\partial Z_{b,L}}{\partial t}+\frac{\partial g_{bx,L}}{\partial x}+\frac{\partial g_{by,L}}{\partial y}=0 \quad (8)$$

$$\gamma'_s\frac{\partial E_m P_{mL}}{\partial t}+\alpha_L\omega_L(S_L-S_L^{*})+\frac{\partial g_{bx,L}}{\partial x}+\frac{\partial g_{by,L}}{\partial y}+\gamma'_s[\varepsilon_1 P_{mL}+(1-\varepsilon_1)P_{mL,0}]\left(\frac{\partial z_b}{\partial t}-\frac{\partial E_m}{\partial t}\right)=0 \quad (9)$$

In above equations: *z*=the water level; *h*=the water depth; *u*, *v*= the vertically averaged velocities in x, y directions, respectively; *t*=the time; *k*= the turbulent kinetic energy; ε =the turbulence dissipation rate; *g*=the acceleration of gravity; *n*=the Manning's coefficient; S_L, S_L^{*}, ω_L, α_L =the *L*-th group sediment concentration, sediment carrying capacity, settling velocity, saturation recovery coefficient, respectively; $Z_{S,L}$ =the deposition thickness of the *L*-th group sediment, γ_s' =the dry bulk density; $Z_{b,L}$, $g_{bx,L}$ and $g_{by,L}$ =deposition thickness, discharge per unit width in x and y directions of the *L*-th group bed load, respectively; P_{mL} and $P_{mL,0}$ =bed material compositions and original bed material composition, respectively; z_b =the bed level, E_m =the thickness of active layer; $\varepsilon_1=0$ (if the original river bed is scoured) or $\varepsilon_1=1$ (if the original

Formatted: Font Alignment: Center

Formatted: Font: Italic

Formatted: Font: Italic

Formatted: Font: Italic

river bed is deposited).

In (1)-(6), the effective viscosity (ν_e) is the sum of the viscosity of water (ν) and the eddy viscosity coefficient of water (ν_t). The values and the calculation of some coefficients such as $\nu_t, P_k, P_{kv}, P_{\varepsilon v}, C_{1\varepsilon}^*, C_\mu, \alpha_k, \alpha_\varepsilon$, can be found in (Yakhot and Orzag, 1986; Rodi 1993).

2.2. Modified ~~plane~~ 2D depth averaged RNG k-ε model in body fitted coordinates

As the river under investigation consists of several irregular bends where strong circulation flow exists, the ~~plane~~ 2D depth averaged RNG k-ε sediment model usually can not reflect the influence of such flow. Therefore, the model needs to be modified to take the influence of circulation flow into account.

To facilitate the description, ~~In body fitted coordinates (BFC),~~ the general control equations of the ~~plane~~ 2D depth averaged RNG *k-ε* sediment model can be written ~~as followings~~in body fitted coordinates (BFC):

$$\frac{\partial}{\partial t}(h\Phi)+\frac{1}{J}\frac{\partial}{\partial \xi}(hU\Phi)+\frac{1}{J}\frac{\partial}{\partial \eta}(hV\Phi)=\frac{1}{J}\frac{\partial}{\partial \xi}(\frac{\alpha h\Gamma_\Phi}{J}\frac{\partial \Phi}{\partial \xi})+\frac{1}{J}\frac{\partial}{\partial \eta}(\frac{\gamma h\Gamma_\Phi}{J}\frac{\partial \Phi}{\partial \eta})+S_\Phi(\xi,\eta) \quad (10)$$

where the general variable Φ represents 1, *u*, *v*, *k*, *ε*, S_L in (1)-(6), respectively; ξ and η = the curvilinear coordinates along river bank direction and perpendicular to the river bank direction, respectively; J, α, β, γ = transformation factors, $J = x_\xi y_\eta - x_\eta y_\xi$, $\alpha = x_\eta^2 + y_\eta^2$, $\beta = x_\xi x_\eta + y_\xi y_\eta$, $\gamma = x_\xi^2 + y_\xi^2$; U and V = components of inverter velocity in ξ and η directions, respectively, $U = uy_\eta - vx_\eta$, $V = -uy_\xi + vx_\xi$; Γ_Φ = general diffusion coefficient; the source terms of the momentum equations (Eq.s (2) and (3)) are as following:

$$S_u = -\frac{1}{J} gh(z_\xi y_\eta - z_\eta y_\xi) - \frac{1}{J}\frac{\partial}{\partial \xi}\left(\frac{\beta \Gamma_u h}{J}\frac{\partial u}{\partial \eta}\right) - \frac{1}{J}\frac{\partial}{\partial \eta}\left(\frac{\beta \Gamma_u h}{J}\frac{\partial u}{\partial \xi}\right) - \frac{gn^2 u\sqrt{u^2+v^2}}{h^{1/3}} \quad (11)$$

$$S_v = -\frac{1}{J} gh(-z_\xi x_\eta + z_\eta x_\xi) - \frac{1}{J}\frac{\partial}{\partial \xi}\left(\frac{\beta \Gamma_v h}{J}\frac{\partial v}{\partial \eta}\right) - \frac{1}{J}\frac{\partial}{\partial \eta}\left(\frac{\beta \Gamma_v h}{J}\frac{\partial v}{\partial \xi}\right) - \frac{gn^2 v\sqrt{u^2+v^2}}{H^{1/3}} \quad (12)$$

To simulate the influence of circulation flow of bend, extra source terms need to be added in the momentum equations. These new source terms are as following (Lien, et al, 1999):

$$S_u^{new} = S_u + M_u \ , \ S_v^{new} = S_v + M_v \quad (13)$$

in which the extra source terms can be calculated by

$$M_u = -\frac{1}{J^2}\frac{u\sqrt{\gamma}}{\sqrt{u^2+v^2}}\frac{\partial}{\partial \eta}\left(|\bar{u}|\bar{u}\phi\right) \ , \ M_v = -\frac{1}{J^2}\frac{v\sqrt{\gamma}}{\sqrt{u^2+v^2}}\frac{\partial}{\partial \eta}\left(|\bar{u}|\bar{u}\phi\right) \quad (14)$$

where $\phi = \sqrt{\frac{\gamma}{\alpha}}\frac{h^2}{R_\eta}k_{TS}$, $\bar{u} = \frac{ux_\xi + vy_\xi}{\sqrt{\gamma}}$, $\bar{v} = \frac{ux_\eta + vy_\eta}{\sqrt{\alpha}}$, ~~$R_\eta$~~ R_η = the curvature radius of the bend, k_{TS}= the lateral exchange coefficient due to circulation flow and can be calculated by

$$k_{TS} = 5\frac{\sqrt{g}}{\kappa C} - 15.6\left(\frac{\sqrt{g}}{\kappa C}\right)^2 + 37.5\left(\frac{\sqrt{g}}{\kappa C}\right)^3 \quad (15)$$

where ~~κ~~ κ= Karman constant which is related to the sediment concentration (see below), C = Chezy coefficient.

$$\kappa = 0.42[1 - 4.2(0.365 - S_v)\sqrt{S_v}] \quad (16)$$

where S_v =the sediment concentration by volume.

~~Before we can apply the above equations for simulation, t~~The following key parameters need to be determined~~.~~ before the model can be applied for simulation.

2.3. Suspended sediment carrying capacity

Considering the effect of sediment concentration on Karman constant and silt deposition, Zhang

Formatted: Font Alignment: Center

Formatted: Right, Font Alignment: Center

and Zhang(1992)presented a semi-empirical and semi-theoretical formula to calculate suspended sediment carrying capacity based on the relationship between the energy consumption of flow and the needed floating power of sediment. Being verified by broad range of measured data, the formula has a high adaptability and can be used in the Upper Yellow River. The total suspended sediment carrying capacity can be calculated as following:

$$S^* = 2.5\left[\frac{(0.0022+S_v)\overline{U}^3}{\kappa\frac{\gamma_s-\gamma_m}{\gamma_m}gh\omega_s}\ln\left(\frac{h}{6D_{50}}\right)\right]^{0.62} \quad (16\text{~~}17)$$

where $\overline{U}$ =the vertical mean velocity; D_{50}=the medium diameter of bed material; γ_s, γ_m =bulk densities of sediment and muddy water, respectively; ω_s =the group setting velocity. The units system adopted is kg, m and s.

The group sediment carrying capacity S_L^* is obtained by multiplying **S*** with p_L^* (the graduation of group sediment carrying capacity):

$$S_L^* = p_L^* S^* \quad (17\text{~~}18)$$

and p_L^* can be calculated by (Zhang,et al. 1988):

$$p_L^* = wp_L + (1-w)p_{bL}' \quad (18\text{~~}19)$$

where P_L=the graduation of suspended sediment at inlet; p_{bL}' =related to the graduation of bed material; w=the weight factor, and its value ranges from 0.62 to 0.85 when the river bed is silted; from 0.64 to 0.86 when the river bed is scoured; and from 0.49 to 0.52 when the river bed keeps the balance of erosion and deposition.

2.4. Sediment setting velocity

Formatted: Font Alignment: Center

Formatted: Font: Not Italic

Formatted: Font: Not Italic

Formatted: Font Alignment: Center

The sediment setting velocity is a very important parameter in the sediment model. There are a lot of formulae to calculate sediment setting velocity, among which the formula developed by Zhang (1988) is one of the most representative formulae that are suitable for the sediment in the Yellow River. According to Zhang (1988), the single grain sediment setting velocity in clean water can be calculated ~~by following formula~~as:

~~$$\omega_0 = \begin{cases} \dfrac{1}{25.6}\dfrac{\gamma_s-\gamma}{\gamma}g\dfrac{d^2}{\nu}, & if\ d \le 0.1mm \\ 1.044\sqrt{\dfrac{\gamma_s-\gamma}{\gamma}gd}, & if\ d \ge 4mm \\ \sqrt{\left(13.95\dfrac{\nu}{d}\right)^2+1.09\dfrac{\gamma_s-\gamma}{\gamma}gd}-C_1\dfrac{\nu}{d}, & if\ 0.1mm < d < 4mm \end{cases}$$~~

$$\omega_0 = \begin{cases} \dfrac{1}{25.6}\dfrac{\gamma_s-\gamma}{\gamma}g\dfrac{d^2}{\nu}, & \text{for } d \le 0.1\text{mm} \\ 1.044\sqrt{\dfrac{\gamma_s-\gamma}{\gamma}gd}, & \text{for } d \ge 4\text{mm} \\ \sqrt{\left(13.95\dfrac{\nu}{d}\right)^2+1.09\dfrac{\gamma_s-\gamma}{\gamma}gd}-C_1\dfrac{\nu}{d}, & \text{for } 0.1\text{mm} < d < 4\text{mm} \end{cases} \quad (~~19~~20)$$

where ω_0 = the sediment setting velocity in clear water, d the diameter of single grain sediment.

The sediment concentration in the Yellow River is usually high, which will affect the sediment setting velocity. Therefore, the formula must be modified to take the effect of sediment concentration into account. According to Zhang and Zhang (1992), the sediment setting velocity in muddy water can be estimated as:

$$\omega = \omega_0\left[\left(1-\frac{S_v}{2.25\sqrt{d_{50}}}\right)^{3.5}(1-1.25S_v)\right] \quad (20)$$

where d_{50} is the medium diameter of a group of sediment.

2.5. Bedload sediment transport rate

Bedload transport rate is an important parameter that can be computed as following (Dou, *et al.* 1995):

$$g_{b,L} = K_0 \frac{\gamma_s U' \overline{U}^3}{\frac{\gamma_s - \gamma}{\gamma} g \omega_L C_0^2} \quad (2122)$$

where K_0=0.001 ;C_0=$h^{1/6}/(ng^{1/2})$;~~$\overline{U}$ = averaged flow velocity,~~ $U' = \begin{cases} \overline{U} - U_c, & \overline{U} > U_c \\ 0, & \overline{U} \le U_c \end{cases}$; ~~U_c~~ U_c

= the incipient velocity of sediment, which can be calculated by:

$$U_c = 0.265 \ln(\frac{11h}{\Delta}) \sqrt{\frac{\gamma_s - \gamma}{\gamma} gd + 0.19 \frac{\varepsilon_k + gh\delta}{d_{b50}}} \quad (2223)$$

in which d_{b50} =the medium bedload diameter; $\varepsilon_k = 2.56 \times 10^{-6} m^3/s^2$; $\delta = 0.12 \times 10^{-6} m$;

Δ = roughness height of rive bed and can be determined as:

$$\Delta = \begin{cases} 0.5mm, & D_{50} \le 0.5mm, \\ D_{50}, & D_{50} > 0.5mm. \end{cases} \quad (2324)$$

2.6. Recovering saturation coefficient

Recovering saturation coefficient in (6) and (7) can be evaluated by (Wei *et al.* 1997)

$$\alpha_L = \begin{cases} 0.001/\omega_L^{0.3}, & S_L \ge S_L^* \\ 0.001/\omega_L^{0.7}, & S_L < S_L^* \end{cases} \quad (254)$$

The above formula is used to calculate the recovering saturation coefficient in (6) and (7).

3. Numerical methods

3.1. Discretization of the control equations

Formatted: Font: Italic

Formatted: Font Alignment: Center

Formatted: Font: Italic

The general control equation ~~of the plane 2D RNG k-ε sediment model in the BFC system is~~ (10) is discretized with ~~, and~~ finite volume method (FVM) (Versteeg~~, et al~~ and Malalasekera 1995). ~~is used to discretize it.~~ The computational domain is rectangular in the BFC system and can be easily divided into a series of small rectangles, as shown in Figure 1. Collocated grid system is adopted in this study. In order to avoid the checkerboard pressure difference, momentum interpolation method (Rhie and Chow, 1983) is used. The representative control volume is ΔV and its centre is node P. The east, west, south and north faces of the control volume are e, w, s and n, respectively. The east, west, south and north neighbor nodes of P are E, W, S and N, respectively. Integrating Eq. (10) over the control volume ΔV yields:

$$\int_{\Delta V}\frac{\partial}{\partial t}(h\Phi)dV+\int_{\Delta V}\frac{1}{J}\frac{\partial}{\partial \xi}(hU\Phi)dV+\int_{\Delta V}\frac{1}{J}\frac{\partial}{\partial \eta}(hV\Phi)dV = \int_{\Delta V}\frac{1}{J}\frac{\partial}{\partial \xi}(\frac{\alpha h\overline{\Gamma}_{\Phi}}{J}\frac{\partial \Phi}{\partial \xi})dV+\int_{\Delta V}\frac{1}{J}\frac{\partial}{\partial \eta}(\frac{\gamma h\overline{\Gamma}_{\Phi}}{J}\frac{\partial \Phi}{\partial \eta})dV+\int_{\Delta V}S_{\Phi}(\xi,\eta)dV \quad (26)$$

The first term (i.e. unsteady term, represented by I_t) on the left hand side is discretized by the first order implicit scheme:

$$I_t \doteq \frac{h_P\Phi_P-h_P^*\Phi_P^*}{\Delta t}J_P\Delta\xi\Delta\eta \quad (27)$$

where $\Delta t, \Delta\xi, \Delta\eta$ are time step, spatial steps in ξ and η directions, respectively. Subscript * represents the variable of the last time step.

The second and third terms (i.e. convective terms, represented by I_C) on the left hand side are discretized using an improved QUICK scheme developed by Hayase, *et al.* (1992). In this scheme, a deferred correction method presented by Khosla and Rubin (1974) is used to improve the

QUICK scheme.

$$I_C = E_e - E_w + E_n - E_s \quad (28)$$

where

$$E_e = [|F_e, 0|]\left(\Phi_P + \frac{1}{8}(3\Phi_E - 2\Phi_P - \Phi_W)^*\right) + [|-F_e, 0|]\left(\Phi_E + \frac{1}{8}(3\Phi_P - 2\Phi_E - \Phi_{EE})^*\right) \quad (29)$$

$$E_w = [|F_w, 0|]\left(\Phi_W + \frac{1}{8}(3\Phi_P - 2\Phi_W - \Phi_{WW})^*\right) + [|-F_w, 0|]\left(\Phi_E + \frac{1}{8}(3\Phi_W - 2\Phi_P - \Phi_E)^*\right) \quad (30)$$

$$E_n = [|F_n, 0|]\left(\Phi_P + \frac{1}{8}(3\Phi_N - 2\Phi_P - \Phi_S)^*\right) + [|-F_n, 0|]\left(\Phi_N + \frac{1}{8}(3\Phi_P - 2\Phi_N - \Phi_{NN})^*\right) \quad (31)$$

$$E_s = [|F_s, 0|]\left(\Phi_S + \frac{1}{8}(3\Phi_P - 2\Phi_S - \Phi_{SS})^*\right) + [|-F_s, 0|]\left(\Phi_P + \frac{1}{8}(3\Phi_S - 2\Phi_P - \Phi_N)^*\right) \quad (32)$$

In which $[|F_e, 0|] = max(F_e, 0)$, $F_e = (hU\Delta\eta)_e$, $F_n = (hV\Delta\xi)_n$.

As a result, the scheme has not only the third order accuracy, but is also diagonally dominant and can be easily programmed.

The first and second terms on the right hand side (i.e. diffusion terms, represented by I_D) are discretized using the second order central difference scheme.

$$I_D = D_e(\Phi_E - \Phi_P) - D_w(\Phi_P - \Phi_W) + D_n(\Phi_N - \Phi_P) - D_s(\Phi_P - \Phi_S) \quad (33)$$

where

$$D_e = \left(\frac{\alpha\Gamma_\Phi h}{J}\right)_e \frac{\Delta\eta}{(\delta\xi)_e} , D_n = \left(\frac{\gamma\Gamma_\Phi h}{J}\right)_n \frac{\Delta\xi}{(\delta\eta)_n} .$$

The last term on the right hand side (the source term, represented by I_S) can be dealt with using the following local linear method:

$$I_{S_\Phi} = I_{S_{\Phi C}} + I_{S_{\Phi P}} \Phi_P \quad (34)$$

where $I_{S_{\Phi P}} \le 0$. As for momentum equations, the source terms are as following:

$$I_{S_{uC}} = -\Delta\xi\Delta\eta\left[gh(z_\xi y_\eta - z_\eta y_\xi) + \frac{\partial}{\partial\xi}\left(\frac{\beta\Gamma_u h}{J}\frac{\partial u}{\partial\eta}\right) + \frac{\partial}{\partial\eta}\left(\frac{\beta\Gamma_u h}{J}\frac{\partial u}{\partial\xi}\right) + \frac{1}{J}\frac{u\sqrt{\gamma}}{\sqrt{u^2+v^2}}\frac{\partial}{\partial\eta}\left(|\bar{u}|\bar{u}\phi\right)\right]$$

$$I_{S_{vC}} = -\Delta\xi\Delta\eta\left[gh(-z_\xi x_\eta + z_\eta x_\xi) + \frac{\partial}{\partial\xi}\left(\frac{\beta\Gamma_v h}{J}\frac{\partial v}{\partial\eta}\right) + \frac{\partial}{\partial\eta}\left(\frac{\beta\Gamma_v h}{J}\frac{\partial v}{\partial\xi}\right) + \frac{1}{J}\frac{v\sqrt{\gamma}}{\sqrt{u^2+v^2}}\frac{\partial}{\partial\eta}\left(|\bar{u}|\bar{u}\phi\right)\right]$$

$$I_{S_{uP}} = I_{S_{vP}} = -\frac{gn^2\sqrt{u^2+v^2}}{h^{1/3}} J_P \Delta\xi\Delta\eta .$$

The discretized equation of the general governing equation (10) using the above discretized scheme is as following:

$$a_P\Phi_P = a_E\Phi_E + a_W\Phi_W + a_N\Phi_N + a_S\Phi_S + I_{S_{\Phi C}} + S^*_{ad} \quad (35)$$

where

$$a_E = D_e + [|-F_e, 0|], a_W = D_w + [|F_w, 0|] \ , \ a_N = D_n + [|-F_n, 0|], a_S = D_s + [|F_s, 0|],$$

$$a_P = a_E + a_W + a_N + a_S + F_e - F_w + F_n - F_s + a^*_P - I_{S_{\Phi P}} , b = a^*_P\Phi^*_P + I_{S_{\Phi C}} ,$$

$$a^*_P = \frac{h^*_P}{\Delta t} J_P\Delta\xi\Delta\eta , \ S^*_{ad} = (S^*_{ad})_e + (S^*_{ad})_w + (S^*_{ad})_n + (S^*_{ad})_s ,$$

$$(S^*_{ad})_e = \frac{1}{8}(3\Phi_E - 2\Phi_P - \Phi_W)^*[|F_e, 0|] + \frac{1}{8}(3\Phi_P - 2\Phi_E - \Phi_{EE})^*[|-F_e, 0|],$$

$$(S^*_{ad})_w = \frac{1}{8}(3\Phi_P - 2\Phi_W - \Phi_{WW})^*[|F_w, 0|] + \frac{1}{8}(3\Phi_W - 2\Phi_P - \Phi_E)^*[|-F_w, 0|],$$

$$(S^*_{ad})_n = \frac{1}{8}(3\Phi_N - 2\Phi_P - \Phi_S)^*[|F_n, 0|] + \frac{1}{8}(3\Phi_P - 2\Phi_N - \Phi_{NN})^*[|-F_n, 0|],$$

$$(S^*_{ad})_s = \frac{1}{8}(3\Phi_P - 2\Phi_S - \Phi_{SS})^*[|F_s, 0|] + \frac{1}{8}(3\Phi_S - 2\Phi_P - \Phi_N)^*[|-F_s, 0|].$$

~~The first term (i.e. unsteady term) on the left hand side is discretized by the first order implicit scheme. The second and third terms (i.e. convective terms) on the left hand side are discretized~~

~~using an improved QUICK scheme developed by Hayase, et al.(1992). In this scheme, a deferred correction method presented by Khosla and Rubin (1974) is used to improve the QUICK scheme. As a result, it is not only diagonally dominant second order accuracy scheme, but also easily programmed. The first and second terms on the right hand side (i.e. diffusion terms) are discretized using the second order central difference scheme.~~ Collocated grids SIMPLEC algorithm in body fitted coordinate system (Van Doormaal and Raithby ~~, et al.~~1984) is used to solve the coupled problem of water level and velocities. The discretized equations are five-diagonal, which can be solved using tridiagonal matrix algorithm (TDMA) (Versteeg and Malalasekera~~, et al.~~ 1995).

3.2. Semi-coupled algorithm for sediment model

~~Generally speaking, the algorithms about numerical simulation of sediment transport and bed deformation can be divided into two types: separated algorithm and coupled algorithm. In the separated algorithm, the sediment module starts after the hydraulic module has started a certain time when the hydraulic elements, such as velocity, water level, have tended to stability. The hydraulic module then stopped after the sediment module starts. The separated algorithm is time saving but not accuracy. This is because that the hydraulic elements cannot update with the change of bed deformation in the algorithm, which may introduce serious error when the riverbed changes greatly. While in coupled algorithm, the flow module and sediment module run together and exchange information every time step. Therefore, the coupled algorithm is more accurate but it is also time consuming.~~

In this study, a semi-coupled algorithm is developed by combining the advantages of coupled and ~~separate~~ decoupled schemes~~algorithms~~. In the process of long time simulation of sediment transport when river bed changes slowly, the bed elevation change each time step has minimal impacts on flow field, therefore, it is unnecessary to update the hydraulic elements each time step. Thus, in order to reduce the computational cost, the hydraulic module runs intermittently while the sediment module keeps running all the time. In the semi-coupled scheme, after the sediment module starts to run, the hydraulic module will stop running for a certain number of time steps (for example, 1000-5000 time steps), then it will run again. After running for certain time steps (such as 60-120 time steps) to update the hydraulic elements, it will then stop running. The process is repeated until the required accuracy is reached.~~In the process of sediment simulation, hydraulic elements usually change very slightly each time step after the flow module has started a certain time steps when the hydraulic elements tend to stability except for high unsteady flow condition. Therefore, it is unnecessary to update the hydraulic elements each time step for such flow. Thus, in order to save computational time, the hydraulic elements are updated after a number of time steps (such as 500-5000 steps), while the sediment elements are updated every time step in the semi-coupled algorithm. In the algorithm, the hydraulic module is working intermittently after the sediment module has started. The hydraulic module keeps running for certain time steps (such as 60-120 time steps) to keep the hydraulic elements tending stability each time when it has started.~~

Let *t* be simulating time, *t0_flow* the initial simulating time for the flow module, ~~*t0_sediment the initial simulating time for the sediment module,*~~ *t1_flow* the flow module working time each time, *t2_flow* the time interval between two adjacent times when flow module is started, ~~*t1_sediment the*~~

Formatted: Font: Italic

Formatted: Font: Italic

Formatted: Font: Italic

Formatted: Font: Italic

~~*sediment module working time each time,*~~ *t_max* the required simulating time, the procedure of this semi-coupled ~~algorithm~~ scheme is detailed as following:

Algorithm of semi-coupled scheme:

Step 1. If *t*≤*t0_flow*, only the hydraulic module is running；

Step 2. If *t0_flow*< *t*<*t_max*, the sediment module is running.~~If t0_flow<t≤t0_flow+t0_sediment, the hydraulic and sediment modules are running together；~~

Step 3. If *t0_flow*< *t*<*t_max*, and mod (*t*, *t2_flow*)<*t1_flow*, the flow and sediment modules are running together；otherwise, only the sediment module is running.

Step 4. If *t*>*t_max*, stop.

~~If t0_flow+t0_sediment< t<t_max, the sediment module is always running, but the flow module is running intermittently. That is to say, every time after the sediment module has been running for t1_sediment, the hydraulic module will begin to run. After it has been running for t1_flow, the hydraulic module is no longer running. In the meantime, the sediment module keeps on running.~~

where *mod* is a function which means modulus and *mod* (*t*, *t2_flow*) is the remainder when t is divided by t2_flow. In this study, time step *dt*=12s, *t0_flow*=5h, ~~*t0_sediment=5h,*~~ *t1_flow*=1h, *t2_flow*=12h~~t1_sediment=12h~~. ~~In the algorithm, the aims of step 1 and step 2 are to keep the simulation process stable.~~ Numerical experiments indicate that the computational time of the semi-coupled ~~algorithm~~ scheme is about 60% of the coupled ~~algorithm~~scheme.

3.3. Boundary and initial conditions

Formatted: Font: Italic

Formatted: Font: Italic

Formatted: Font: Italic

Formatted: Font: Italic

We choose two adjacent field measurements to verify the sediment model. ~~Water discharge and sediment concentration are given at the inlet based on values interpolated by field data measured~~ The field measurements were conducted on December 6, 2008 and on July 17, 2009, respectively. The time interval between the two measurements is 203 days. Water discharge and sediment concentration are given at the inlet based on values interpolated by field data measured on December 6, 2008 and on July 17, 2009. The turbulence kinetic energy (k) and its dissipation rate (ε) at the inlet are calculated using empirical formulae (Rodi 1993). On the water outlet boundary, water level ~~is~~ specified set based on values by interpolating the field data measured on December 6, 2008 and on July 17, 2009. Other variables are dealt with fully developed condition. On the wall boundary, no-slip boundary condition is applied. The velocity parallel to the river bank at the first cell is estimated using standard wall function (Guo, *et al.* 2008).

Formatted: Font: Italic

Formatted: Font: Italic

Formatted: Font: Italic

In order to study the flow and sediment transport in the studied reach, four cases are set based on discharge and sediment concentration at the inlet. The boundary conditions of the four cases are presented in Table 1. Case 1 is set according to the field measured data on December 6, 2008, while Case 2 is set according to the data measured on July 17, 2009. Case 3 and Case 4 are set according to the hydrological data in the past years. Cases 1 and 4 represents the hydraulic conditions of the dry and flood seasons, respectively, while Cases 2 and 3 represents the hydraulic condition of the wet season.

The initial values are based on field measured data on December 6, 2008~~.~~, including the position of cross-sections, water level, maximum water depth, average water depth, river width, average

velocity of 14 cross-sections (see Table 2). ~~Figure 1 shows the contour of the initial relative bed elevation of the computational domain, and the absolute bed elevation (the Yellow Sea elevation) is the relative value added by 1200m.~~ The initial water level at each grid is set as the same as the water level at the outlet. u, v and S_L at each grid are set as zero, except for that at the grids at the inlet. However, k and ε can not be set as zero, otherwise, the simulation process will stop unexpected or be unstable. In the simulations, the initial values of k and ε are set as 0.1 m^2/s^2 and 0.0001 m^2/s^2, respectively, based on the authors' experience.~~.~~

The suspended and bedload sediment on the inlet section is divided into three groups with the medium diameter being 0.0249 *mm* and 10 *mm*, respectively. The representative diameters and related percentage for both suspended and bedload sediment are listed in Table ~~2~~3. The bed material is divided into six groups, whose representative diameters and their percent content are presented in Table ~~2~~3. The initial percentage contents of the suspended and bedload are set as the same as the values at the inlet. Some representative diameters of the initial bed material of the whole reach are: d_{50} =10 mm, d_m =15.5 mm, $d_{25}=1$ mm, $d_{35}=4$ mm, $d_{75}=20$ mm, $d_{90}=70$ mm and $d_{95}=100$ mm, where d_m = the mean diameter, d_a = the sediment diameter that a% is less than that in the size gradation curve (a=25, 35,50,75,90,95).

3.4. Mesh generation

In the computational domain, along longitudinal direction (ξ-direction), 131 grids are assigned, while along transverse direction (η-direction), 31 grids are set. Poisson equation method is used to make body-fitted coordinate transformation and grid generation (Versteeg, et al. 1995). The total

Formatted: Font: Italic
Formatted: Font: Italic
Formatted: Font: Italic
Formatted: Font: Italic
Formatted: Font: Not Italic
Formatted: Font: Not Italic

number of grids and cells are 4991 and 4800, respectively. To better fit the complex boundary, non-uniform meshes with arbitrarily spatially dependent size were used. This allows for locally refining the concerned regions (e.g. near bends) with small meshes and has the advantage of flexibly assigning meshes in the computational domain. Along transverse direction, there are 30 cells, in which 5 non-uniform cells near left bank and near right bank, respectively. The gird length of the 5 cells near bank increases from bank to interior. Figure 2 shows the mesh distribution near banks and bends.

4. Results and discussions

4.1. Description of the numerical simulation

The Shapotou Reservoir in the Yellow River is located in Ningxia Hui Autonomous Region in China. The studied reach is about 13.4km long, as shown in Figure ~~2~~3. Twenty cross-sections (e.g. SH1-SH15, SHJ1-SHJ5) are assigned in the studied reach, in which SH15 is the inlet, and SH1 is the outlet. The studied reach consists of five bends: Bend A (from SH15 to SH13), Bend B (from SH13 to SH11), Bend C (from SH11 to SH7), Bend D (from SH7 to SH2) and Bend E (from SH2 to SH1). Bends A and B are near the exit of the Heishan Gorge, where the river is deep and narrow, and the current is rapid. The averaged water width at bend A and Bend B is about 135m with the normal water level gradient being about 0.03%. Bends C, D and E are near the Shapotou Dam, where the river is wide and shallow (the averaged water width is about 300 m), and the current is slow. The normal water level gradient is about 0.006% .

In the simulation, the semi-coupled algorithm about flow and sediment modules in the plane 2D

RNG k-ε sediment model is applied. The software of Matlab 7.1 is used to program, and the numerical simulation is conducted in an IBM work station. The CPU of the work station is two cores Intel ® Xeon 2.0G Hz; the memory is 4.0GB; the operation system is Ghost-Server2003 SP2. Typical numerical simulation takes about 16 days.

4.2. Sediment setting velocity

The sediment setting velocities of the six representative groups in the studied reach are calculated by (19) and modified by (20), as shown in Table ~~3~~4.

The sediment setting velocity is affected by the sediment concentration. Here we assume that the sediment concentration is S=10kg/m^3 and the sediment concentration by volume is $S_v=S/\rho_s$=0.038 (ρ_s = density of sediment=2650kg/m^3). It is seen that the same sediment concentration has different influence for the setting velocity of various grain size groups. The correction rate is bigger for fine sediment than that for coarse sediment. In other words, sediment concentration has larger influence for fine sediment than for the coarse one.

4.3. Suspended sediment carrying capacity

The suspended sediment carrying capacity is calculated using (~~16~~17) and (~~17~~18) for different group sediment carrying capacity. Because the numerical results about suspended sediment carrying capacity of the four cases are similar, only the result under the condition of Case 2 is presented in this paper. Figure ~~3~~ 4 shows the distribution of the sediment concentration, the total and the group suspended sediment carrying capacities along the centerline of the studied river

reach. As shown in Figure ~~3~~4, both the total and the group sediment carrying capacity decrease along the way as a whole. It can also be found that the carrying capacity of the second sediment group is the largest among the three sediment groups, while the carrying capacity of the third sediment group is the smallest, which is consistent with the sediment concentration of the three groups at the inlet.

4.4. Bedload sediment transport rate

In this study, four different methods are applied to calculate bedload sediment transport. The first method (Method I) is to calculate group bedload transport rate by (~~21~~22), then summing them together to obtain the total transport rate. The second method (Method II) is to calculate ω by (~~19~~20) and (~~20~~21), where the representative sediment diameter (d) is chosen as d_{35}; then replacing ω_L with ω in (21) to calculate the total bedload sediment transport rate. The third method (Method III) is the same as Method II, except that the representative sediment diameter is d_m. The fourth method (Method IV) is the same as Method II, except that d_{50} is chosen as the representative sediment diameter.

From Table ~~4~~5, it can be seen that the bedload transport rates calculated using the four methods are different. Generally speaking, for non-uniform bedload sediment, it would be more accurate to divide bedload sediment into several groups when computing its transport rate. Therefore, the result calculated using Method I is most reliable. The result calculated by Method II is closer to the result of Method I, indicating that the transport rate of non-uniform bedload sediments can be calculated using the formula for computing the transport rate of uniform bedload sediments when

the representative sediment diameter is chosen as d_{35} for the flow and sediment conditions investigated here. ~~.~~ This result is consistent with the conclusion of Einstein (Zhang, 1988).

4.5. Comparison between measured and calculated velocities

Figure ~~4~~ 5 shows the comparison of the simulated and field measured (on July 16 2009) depth averaged velocities on three selected cross-sections, i.e. SH7, SH5, SHJ2. which are near the inlet, apex, and outlet of Bend D, respectively. Figure 5(1) also shows the comparison of the depth averaged velocities calculated using two methods: Simulation 1 and Simulation 2. In Simulation 1, the circulation flow is not taken into account, while this has been taken into account in Simulation 2. It is seen that the simulated velocity using the second approach is better compared to the measured data than that using the first method, indicating that the modified plane 2D RNG k-ε model is capable of simulating the effect of the circulation flow in natural rivers. ~~Good agreement between numerical calculation and measurements indicates that the modified plane 2D RNG k- ε model is capable of simulating the flow in natural rivers with continuous curves.~~ In general, good agreements between simulated and field measured velocities at three cross sections are obtained.

4.6. Comparison between measured and calculated river bed deformation

~~In~~ Figure ~~5~~6 is~~,~~ the plot of the simulated and field measured (on July 17 2009 bed elevation along the longitudinal direction ~~is compared with field data measured on July 17 2009~~. It is seen that the simulated bed elevation is in good agreement with the measured data. From SH11 to SH9, the river bed is scoured, while from SHJ5 to SH2, the river bed is deposited. The deposit thickness varies significantly from SH2 to SH5 with the largest deposition taking place in SH2 (where the

Formatted: Space Before: 12 pt

514 average deposit thickness is over 1 m), while little deposit takes place at SH5 (where the average
515 deposit thickness is only about 0.01 m).
516
517 In Figure ~~6~~7, the measured and the simulated bed elevations on three typical cross sections are
518 plotted. The three cross sections are SH10, SHJ5 and SH7, which are near the inlet, the bend apex,
519 and the outlet of Bend C, respectively. It is seen from Figure ~~6~~ 7 that the simulated bed elevation
520 agrees well with the measured data on these cross sections, indicating that the ~~plane~~ 2D depth
521 averaged RNG k-ε sediment model can reasonably simulate the bed deformation in the studied
522 reach. The bed on SH10 is scoured as a whole except some tiny areas near the river banks. The
523 bed near the left bank of SHJ5 and SH7 is deposited and the bed near the right bank of the two
524 cross-sections is scoured. Because the left bank is the convex bank , while the right bank is the
525 concave bank in Bend C, the above phenomenon is in consistence with the general rule of
526 sediment transport in a bend.
527
528 ***4.7. Suspended sediment transport***
529 Figure ~~7~~ 8 shows the distribution of suspended sediment concentration along the centerline of the
530 studied reach under the condition of Case 2 with the sediment concentration at the inlet being set
531 as 0.51, 3.53, 10 and 20 kg/m^3, respectively. From Figure ~~7~~8, it is seen that the suspended
532 sediment concentration in the studied reach increases with increasing the suspended sediment
533 concentration at the inlet. As the river of the studied reach becomes wider and shallower as the
534 current moves downstream, the current becomes slower and the sediment carrying capacity
535 becomes weaker accordingly along the way, leading to the decrease of the suspended sediment

concentration along the way.

4.8. The effect of discharge on river bed deformation

In order to investigate the effect of the discharge at the inlet on the bed deformation, numerical simulations were conducted for four cases. The conditions of the four cases are shown in Table 1 except that the sediment concentration at the inlet is set as 3.53kg/m^3. Figure ~~8~~ 9 shows the simulated bed elevation after 10 days development for all four cases. The bed is deposited near the inlet for Cases 1 and 2, while the bed is scoured near the inlet under the condition of Cases 3 and 4. The reason is that the average velocities for the Cases 1 and 2 are small, and the suspended sediment capacities are smaller than the sediment concentration. As a result, the bed is deposited near the inlet. However, after current moves a certain distance, a balance between deposition and scour is reached. The position of balance is about 9.5km from the inlet for Case 1, and it is near SH5; while for Case 2, it is about 10.5km from the inlet and near SH4. The discharges and average velocities of the Cases 3 and 4 are larger, and the suspended sediment capacities of the two cases are larger than sediment concentration. Therefore, the bed is scoured near the inlet. Similar to Cases 1 and 2, a balance between deposition and scour is reached after the current leaves the inlet a certain distance. For Case 3, the position is about 4.5km from the inlet and near SH10; while for Case 4, the position is about 6km from the inlet and near SH9. From above analysis, it can be concluded that the discharge at the inlet has significant influence on the bed deformation near the inlet. However, after the current moves a certain distance, the influence becomes weaker and weaker.

4.9. River bed deformation caused by bedload sediment

Though the bed deformation is mainly caused by the suspended sediment transport, the bedload sediment transport can also have significant effect on the bed deformation for some certain situation. The numerical simulation is conducted under the conditions of the four cases with the sediment concentration at the inlet being 3.53kg/m^3. Figure ~~9~~ 10 shows the percentage of the absolute thickness deposited or scoured by suspended and bedload sediments for four typical cases after 10 days development, respectively. It can be seen that the thicknesses deposited or scoured due to the suspended or bedload sediment transport is quite different. In Cases 1 and 2, the percentage of bed deformation caused by bedload sediment is less than 1%, which can be neglected. In Case 3, the percentage is less than 3% and is still very small and can be neglected. In Case 4, the percentage is about 10%, which can not be neglected Therefore, it can be concluded that the bed deformation caused by bedload sediment can be neglected when the discharge at the inlet is small (less than 1500m^3/s in this study). When the discharge at the inlet is larger (more than 2000m^3/s in this study), however, ~~However,~~ the bed deformation caused by bedload sediment ~~can not~~has to be ~~neglected~~ taken into account.~~when the discharge at the inlet is larger (more than 2000m^3/s).~~

4.10. The variation of effective bed material ~~composition~~granularity

Bed material becomes finer or coarser when the bed is deposited or scoured and it is worth of investigating. Because the simulated results for four cases are similar ~~for the four cases~~, only the numerical result of Case 4 is presented and discussed in this paper. Under the condition of Case 4,

numerical simulations were conducted for the sediment concentration at the inlet (S_{in}) being 0.51kg/m^3 and 10kg/m^3, respectively.

Figure ~~10~~ 11 shows the variation of effective bed material ~~composition~~ granularity along the ~~way~~ river flow direction after 20 days. ~~under the condition of Case 4.~~ In Figure ~~10~~11, the axis x is the distance from the inlet, and the axis y is the percentage of each group effective bed materials. The percentage of the initial bed material for the six groups is 0.2%, 3.8%, 17.9%, 12.7%, 36.5%, 28.9%, respectively~~.~~, as shown by the dash line in Figure 11.

When S_{in} = 0.51kg/m^3, the river bed is scoured as a whole and the bed material size gradation changed after 20 days' scouring. In Figure ~~10~~11(a), it is seen that the percentage of the first three groups(Groups 1-3) of bed material decreased compared the initial value, especially for Groups 2 and 3. The decreasing tendency becomes weaker with the distance and reaches the minimum at the distance of 8.5km from the inlet (near SH6). ~~; m~~Meanwhile, the percentage of the last three groups (Groups 4-6) of bed material increased compared with the initial value. This means that the bed material composition will become coarser when the bed is scouring. However, after SH6, the sediment concentration at the inlet has little influence to the bed deformation and variation of bed material granularity, as shown by Figure 9 and Figure 11.

When S_{in}=10kg/m^3, the situation is different and complicated. ~~bed is deposited as a whole. As~~ As shown in Figure ~~10~~11(b), the bed material percentage of ~~the first three groups~~Groups 1-3 ~~of the bed material~~ increases, while the percentage of Groups 4-6 ~~last three groups of the bed material~~ as

Formatted: Font: Italic

Formatted: Font: Italic

a whole compared with the initial value. ~~decreases. Therefore, if the river bed is deposited, the bed material composition becomes finer.~~ In Figure 11(b), it can also be found that the percentage of the first three groups of the bed material increases with the distance and reaches the maximum near SH6. The percentage of these groups then decreases with the distance. To the contrary, the last three groups of the bed material decreases with the distance and reaches the minimum near SH6 and increases again to the outlet. This means that the river bed becomes finer compared with the initial value when it is deposited. Similar to the condition when S_{in}=0.51 kg/m^3, after SH6, the sediment concentration at the inlet has little influence to the bed deformation and variation of bed material granularity.

~~In Figure 10(a) and Figure 10(b), it is also seen that the first three groups of bed material increases, while the last three groups decreases along the way. Therefore, it is concluded that the bed material becomes finer and finer along the way in the studied reach.~~

5. Conclusions

In this study, a ~~plane~~ 2D depth averaged RNG k-ε sediment model ~~integrated~~ including the effects of secondary currents is developed, which considers the effects of the non-uniform suspended and bedload sediment transport on the bed deformation. In the model, the variation of effective bed material ~~size distribution~~granularity is included. A semi-coupled ~~algorithm~~ scheme is developed by combining the coupled and ~~separate algorithms~~decouple schemes to improve the accuracy of the numerical simulation (comparing with ~~separate algorithms~~the decoupled scheme) and save computational time (comparing with the coupled scheme~~coupled algorithms~~). A series of

Formatted: Font: Italic

numerical simulations have been performed for four typical cases to investigate the sediment transport and bed deformation in the upper reach of the Yellow River. Comparison between the numerical results and field measurements indicates that the ~~plane~~ 2D depth averaged RNG k-ε sediment model can reasonably simulate the sediment transport and the resultant bed deformation of rivers with continuous bends. River bed deformation induced by suspended and bedload sediment transports has been investigated. It is found that the bed deformation caused by bedload sediment transport can be neglected when the discharge at the inlet is small (less than 1500m^3/s in this study). The results also show that the discharge at the inlet has large influence on the bed deformation near the inlet. The influence, however, becomes weaker as the flow moves downstream.

The variation of effective bed material composition has been examined. It is concluded that the bed material composition becomes finer when the bed is deposited. When the bed is scoured, the bed material composition becomes coarser. The bed material composition becomes finer along the way in the studied reach no matter it is deposited or scoured. The sediment concentration at the inlet has significant influence for bed material granularity near the inlet. However, the influence becomes weaker with the distance from the inlet.

Formatted: Font: Italic

6. Acknowledgements

The authors acknowledge with thanks of the following institutes for assisting this study: Ningmeng Hydrographic & Water Resource Office of Yellow River Water Conservancy Committee of China, and Ningxia Shapotou Hydraulic Power Plant of China. Constructive

comments and suggestions from the Editor and Reviewers have greatly improved the quality of the paper.

7. References

~~Bui, M.D., Rutschmann, P., 2010. Numerical modelling of non-equilibrium graded sediment transport in a curved open channel. *Computers & Geosciences*, 36: 792–800.~~

~~Chen, R.F., 1986. Modeling of esturay hydrodynamics-A mixtures of arc and science. *Proceedings of 3rd Inter. Symp. on River Sedimentation*, the University of Mississippi.~~

Dou, G.R., Dong, F.W., Dou, X.P., Li, T.L., 1995. Mathematical modeling of sediment transport in estuaries and coastal regions. *Science in China(Series A)*, 38 (10):1251-1260.

Duan, J.G., Nanda, S.K., 2006. Two-dimensional depth-averaged model simulation of suspended sediment concentration distribution in a groyne field. *Journal of Hydrology*, 327, 426-437.

Duan, J.G., Julien, P.Y., 2010. Numerical simulation of meandering evolution. *Journal of Hydrology*, 391: 34-46.

Falconer, R.A. 1992. Flow and water quality modelling in coastal and inland water. *J. Hydraul. Res.*, 30, 437-452.~~Feldman, A.D., 1981. *HEC models for water resources system simulation: theory and experience*. The Hydraulic Engineering Center, Davis, California.~~

Guo, Y.K., Wang, P.Y., Zhou, H., 2007. Numerical modelling of the flow past irregularities in a pressure conduit, *ASCE J. Hydr. Eng.*, 133(6): 698-702.

Guo, Y.K., Zhang, L.X., Shen, Y.M., Zhang, J.S., 2008. Modeling study of free overfall in a

rectangular channel with strip roughness, *ASCE J. Hydr. Eng.*, 134(5): 664–667.

Guo, Y.K., Wu, X.G., Pan, C.H., Zhang, J., 2012. Numerical Simulation of the Tidal Flow and Suspended Sediment Transport in the Qiantang Estuary, *ASCE Journal of Waterway, Port, Coastal and Ocean Engineering*, 138: 192-203.

Hayase, T., Humphrey, J.A.C., Greif, G., 1992. A consistently formulated QUICK scheme for fast and stable convergence using finite volume iterative calculation proceeding. *J. Comput. Phys.*, 98:108-118.

Hung, M.C., Hsieh, T,Y,, Wu, C.H., Yang, J.C., 2009. Two-Dimensional nonequilibrium noncohesive and cohesive sediment transport model. *J. Hydr. Eng.(ASCE)*, 135(5) : 369-382

Jing, H.F., Guo, Y.K., Li, C.G., Zhang, J.S., 2009. Three-dimensional numerical simulation of compound meandering open channel flow by the Reynolds stress model. *Int. J. Numer. Mech. Fluids*, 59, 927-943.

Jing, H.F., Li, C.G., Guo, Y.K., Xu, W.L., 2011. Numerical simulation of turbulent flows in trapezoidal meandering compound open channels. *Int. J. Numer. Mech. Fluids*, 65, 1071-1083.

Khosla, P.K., Rubin, S.G., 1974. A diagonally dominant second order accurate implicit scheme. *Computer & Fluids*, 2:207-209.

Li, S.S., Millar, R.G., 2011. A two-dimensional morphodynamic model of gravel-bed river with floodplain vegetation. *Earth Surface Process and Landforms*, 36(2): 190-202.

Lien, H.C., Hsieh, T.Y., Yang, J.C., Yeh, K.C., 1999. Bend-flow simulation using 2D depth-averaged model. *ASCE J. Hydr. Eng.*, 125, 1097-1108.

~~Khosla, P.K., Rubin, S.G., 1974. A diagonally dominant second order accurate implicit scheme. *Compute Fluids*, 2:207-209.~~

690 Nagata, N., Hosoda, T., Muramoto, Y., 2000. Numerical analysis of river channel processes with
691 bank erosion. *ASCE J. Hydr. Eng.*, 126 (4): 243 -252.
692 ~~Papanicolaou, A.N., Elhakeem, M., Krallis, G., Prakash, S., Edinger, J., 2008. Sediment Transport~~
693 ~~Modeling Review-Current and Future Developments. *ASCE J. Hydr. Eng.*, 134(1): 1 – 14.~~
694 Rhie, C.M., Chow, W.L., 1983. A numerical study of the turbulent flow past an isolated airfoil
695 with trailing edge separation. *AAIA J.*, 21:1525-1532.
696 ~~Rahman, M.M., Arya, D.S., Geol, N.K., Dhamy, A.P., 2011. Design flow and stage computations~~
697 ~~in the Teesta River, Bangladesh, using frequencey analysis and MIKE 11 modeling. *ASCE J.*~~
698 ~~*Hydrol. Eng.*, 16 (2):176-186.~~
699 Rodi, W., 1993. Turbulence models and their application in hydraulics: A state-of-the-art review,
700 3rd Ed., Balkema, Rotterdam, the Netherlands.
701 ~~Ruther, N., Olsen, N.R.B., 2005. Three-dimensional modeling sediment transport in a narrow~~
702 ~~channel bend. *ASCE J. Hydr. Eng.*, 131 (10): 917-920.~~
703 Serrano-Pacheco, A., Murillo, J., Garcia-Navarro, P., 2012. Finite volumes for 2D shallow-water
704 flow with bed-load transport on unstructured grids, *Journal of Hydraulic Research*, 50(2):
705 154-163.
706 Van Doormaal, J.P., Raithby, G.D., 1984. Enhancement of SIMPLE method for predicting
707 incompressible fluid flows. *Numer. Heat Transfer*, 7(2): 147-163.
708 Versteeg, H.K., Malalasekera, W., 1995. *An introduction to computational fluid dynamics*.
709 Addison Wesley Longman Limited, England.
710 Wei, Z.L., Zhao, L.K., Fu, X.P., 1997. Research on Mathematical Model for Sediment in Yellow
711 River, *J. Wuhan University of Hydro. & Electric Eng.*, 30(5):21-25.

712 Yakhot, V., Orzag, S.A., 1986. Renomalization group analysis of turbulence: basic theory. *J.*
713 *Scient Comput.*, 1, 3-11.
714 Zhang, H.W., Zhang, Q., 1992. Formula of Sediment Carrying Capacity of the Yellow River .
715 *Yellow River*, (11):6-9.
716 Zhang, R.J., 1988. *River Sediment Dynamics(the second edition)*. Beijing: Water Conserversy and
717 Hydropower of China.
718

Table

Click here to download Table: Tables_Jing_R1.doc

Table 1 Boundary conditions of four cases

Cases	Inlet					Outlet
	Q（m^3/s）	U（m/s）	S（kg/m^3）	$k(m^2/s^2)$	$\varepsilon(m^2/s^3)$	z(m)
Case 1	513.50	1.0398	0.51	0.0121	0.0005	1239.68
Case 2	930.00	1.5405	3.53	0.0269	0.0013	1240.65
Case 3	1500.00	1.8098	10	0.0378	0.0016	1241.50
Case 4	2000.00	2.0579	20	0.0492	0.0020	1242.00

Table 2. Some data measured on December 6, 2008

Cross section No.	Distance from the inlet /km	Water level /m	Maximum water depth /m	Average water depth/m	River width /m	Average velocity /m/s
SH2	12.52	1240.51	8.58	6.19	212.10	0.35
SH3	11.71	1240.53	6.10	5.31	269.50	0.31
SHJ2	11.26	1240.54	5.78	5.40	267.50	0.33
SH4	10.58	1240.58	6.70	5.47	215.50	0.49
SHJ3	10.14	1240.76	8.43	5.28	214.90	0.52
SH5	9.68	1240.79	8.47	5.07	228.00	0.56
SH6	8.70	1240.82	7.14	4.47	295.40	0.44
SHJ4	8.20	1240.86	6.23	4.69	259.30	0.49
SH7	7.60	1240.88	6.49	4.75	234.20	0.38
SH8	6.75	1240.90	7.34	5.44	221.70	0.35
SHJ5	6.25	1240.91	6.04	4.72	245.90	0.53
SH9	5.55	1241.02	6.45	4.84	175.90	0.54
SH10	4.69	1241.27	13.68	7.67	115.00	0.44
SH11	3.70	1241.38	6.29	4.65	155.90	0.81

Table 3 The initial percent content of bed materials, suspended sediment and bedload

group	1	2	3	4	5	6
diameters /mm	0.01	0.05	0.25	2	10	40
Bed materials /%	0.2	3.8	17.9	12.7	36.5	28.9
Suspended sediment /%	38	53	9			
Bedload /%				38.3	31.3	30.4

Table 4 Sediment group setting velocity of six groups

Sediment grain size /mm	Single setting velocity (cm/s)	Group setting velocity (cm/s)	Correction rate (%)
0.01	0.0062	0.0059	4.92
0.05	0.1570	0.1522	3.14
0.25	1.6142	1.5877	1.69
2	5.8798	5.8277	0.91
10	13.3038	13.2164	0.67
40	26.6075	26.4575	0.58

Table 5 Bedload sediment transport rate at the centerline of some cross sections calculated by four methods under the condition of Case 2 (unit: kg/ms)

Cross sections	Method I	Method II	Method III	Method IV
SH1	0.0018	0.0023	0	0
SH2	0.0006	0.0003	0	0
SHJ2	0.0013	0.0014	0	0
SHJ3	0.0003	0	0	0
SH6	0.001	0.001	0	0
SH7	0.0033	0.0046	0	0
SHJ5	0.0028	0.0037	0	0
SH10	0.0111	0.013	0.0001	0.0034
SH12	0.0499	0.0523	0.0128	0.0228
SH14	0.0415	0.0439	0.0099	0.0184

Figure 1

Click here to download high resolution image

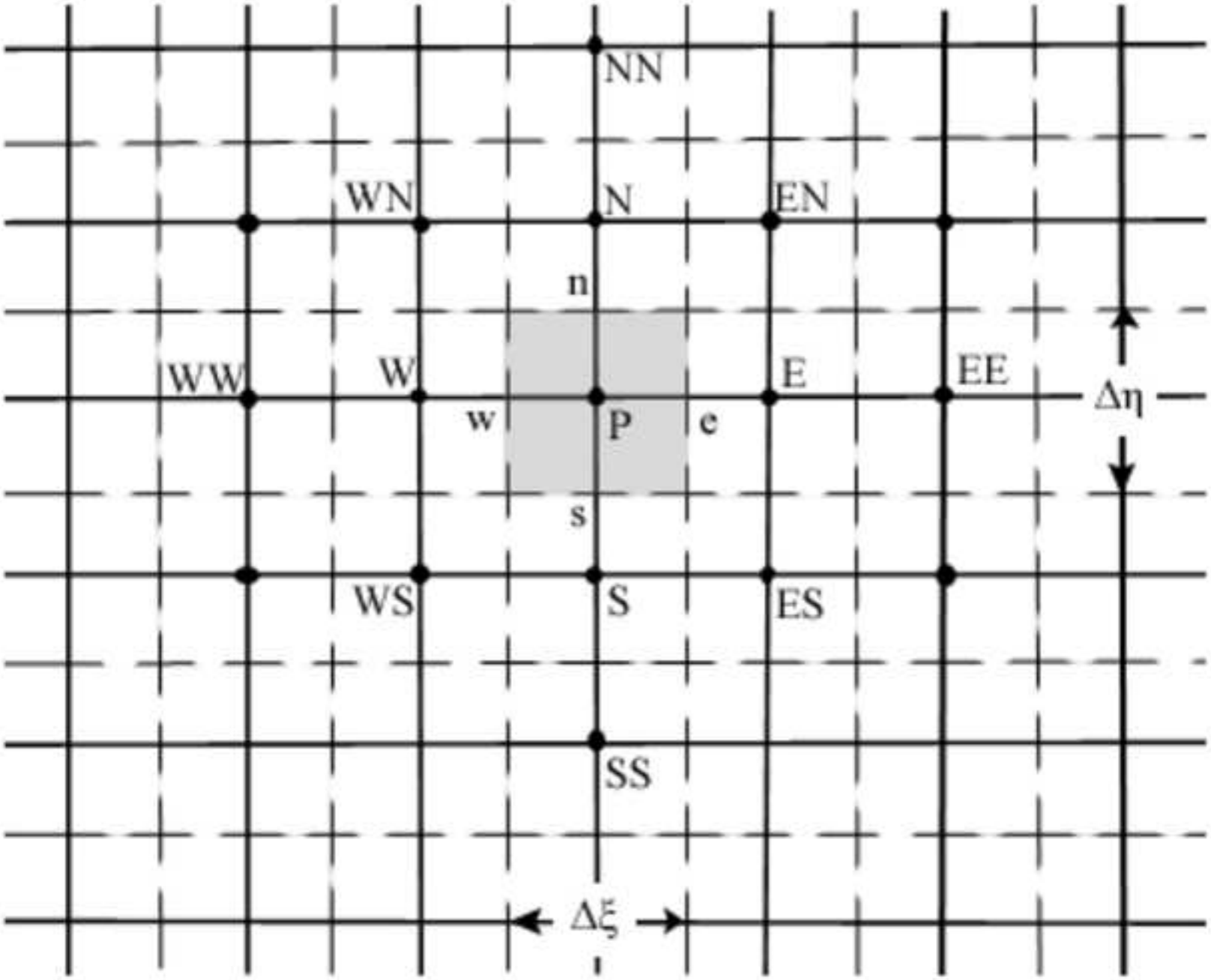

Figure 2

Click here to download high resolution image

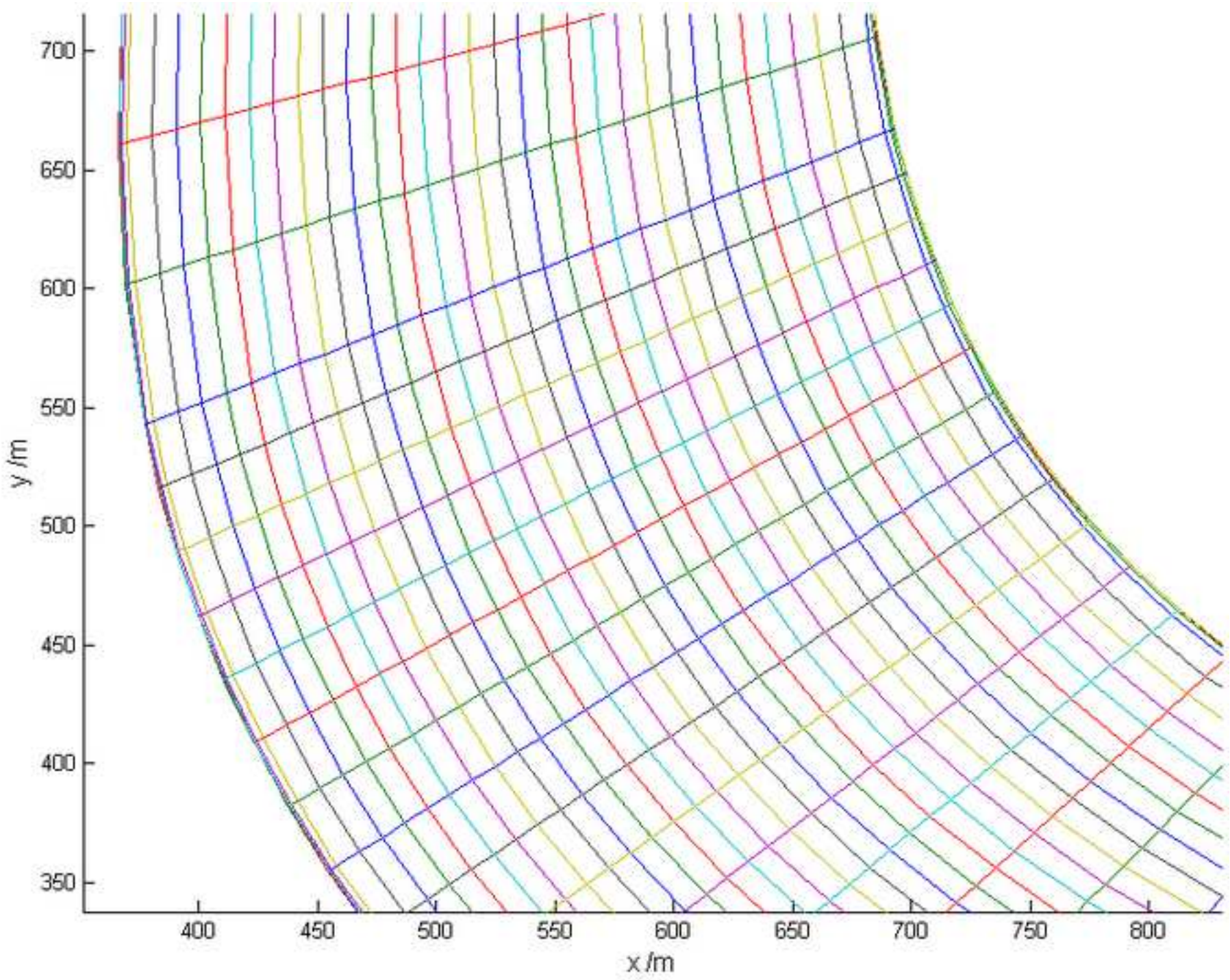

Figure 3

Click here to download high resolution image

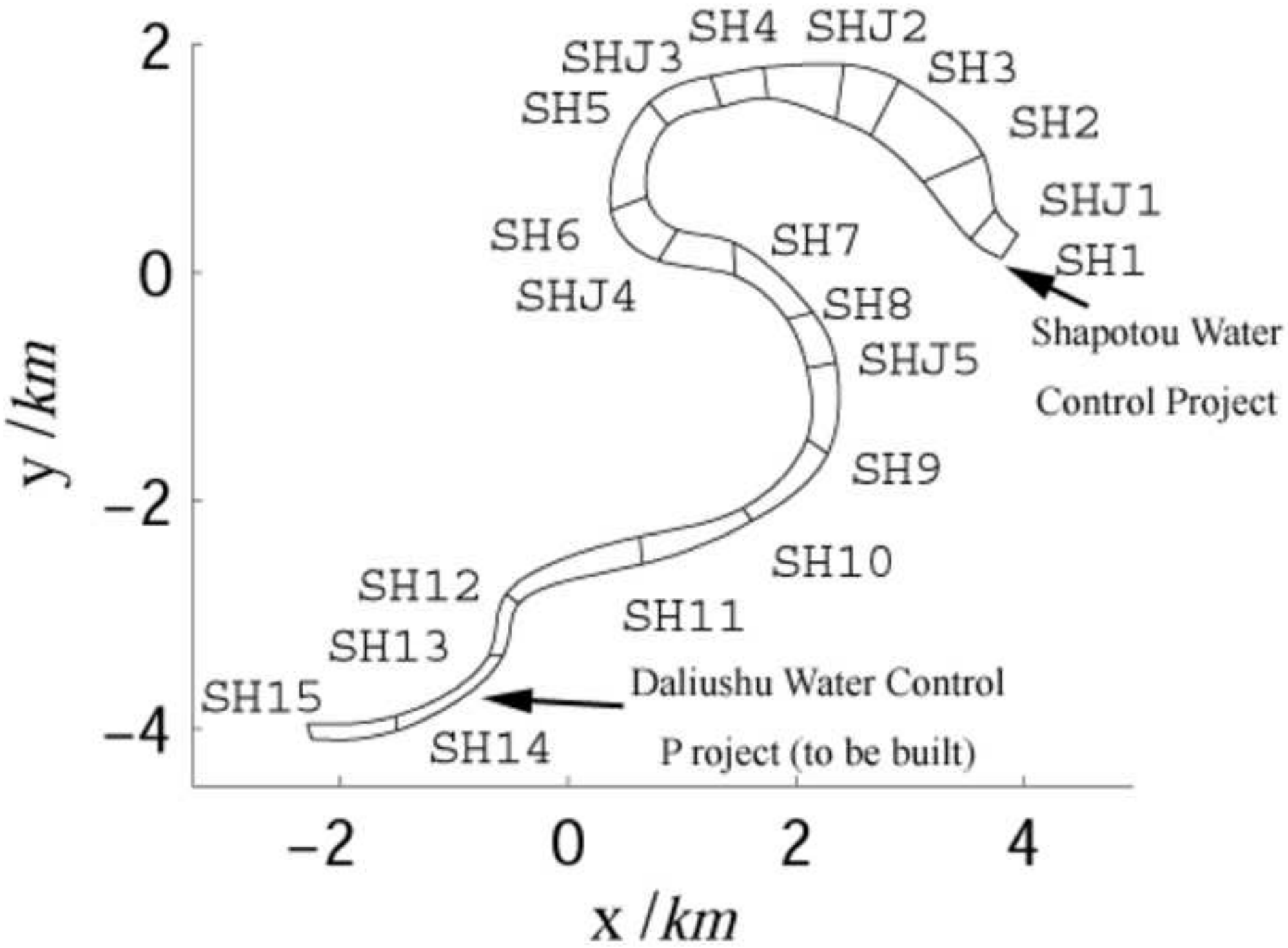

Figure 4

Click here to download high resolution image

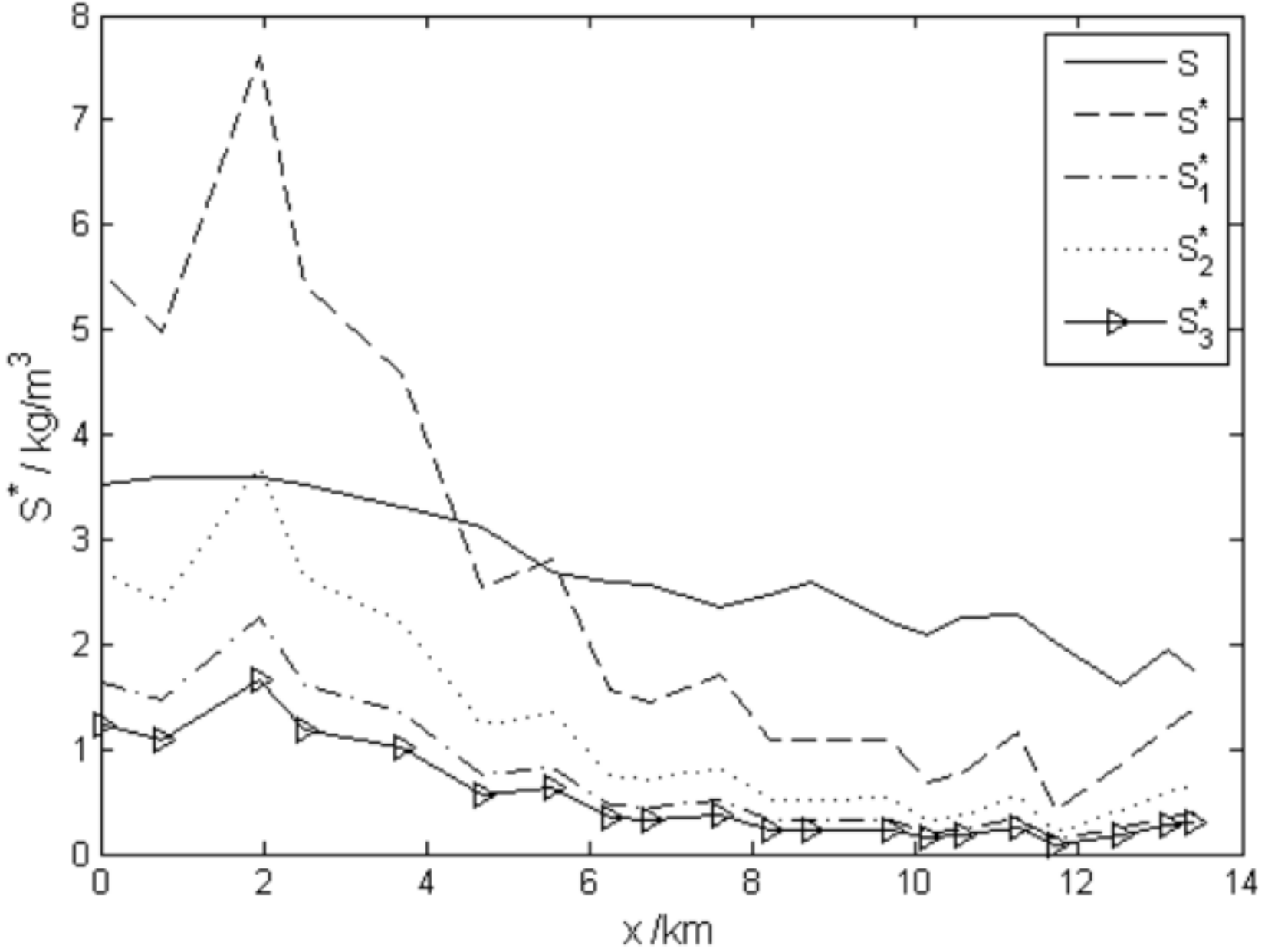

Figure 5(1)
Click here to download high resolution image

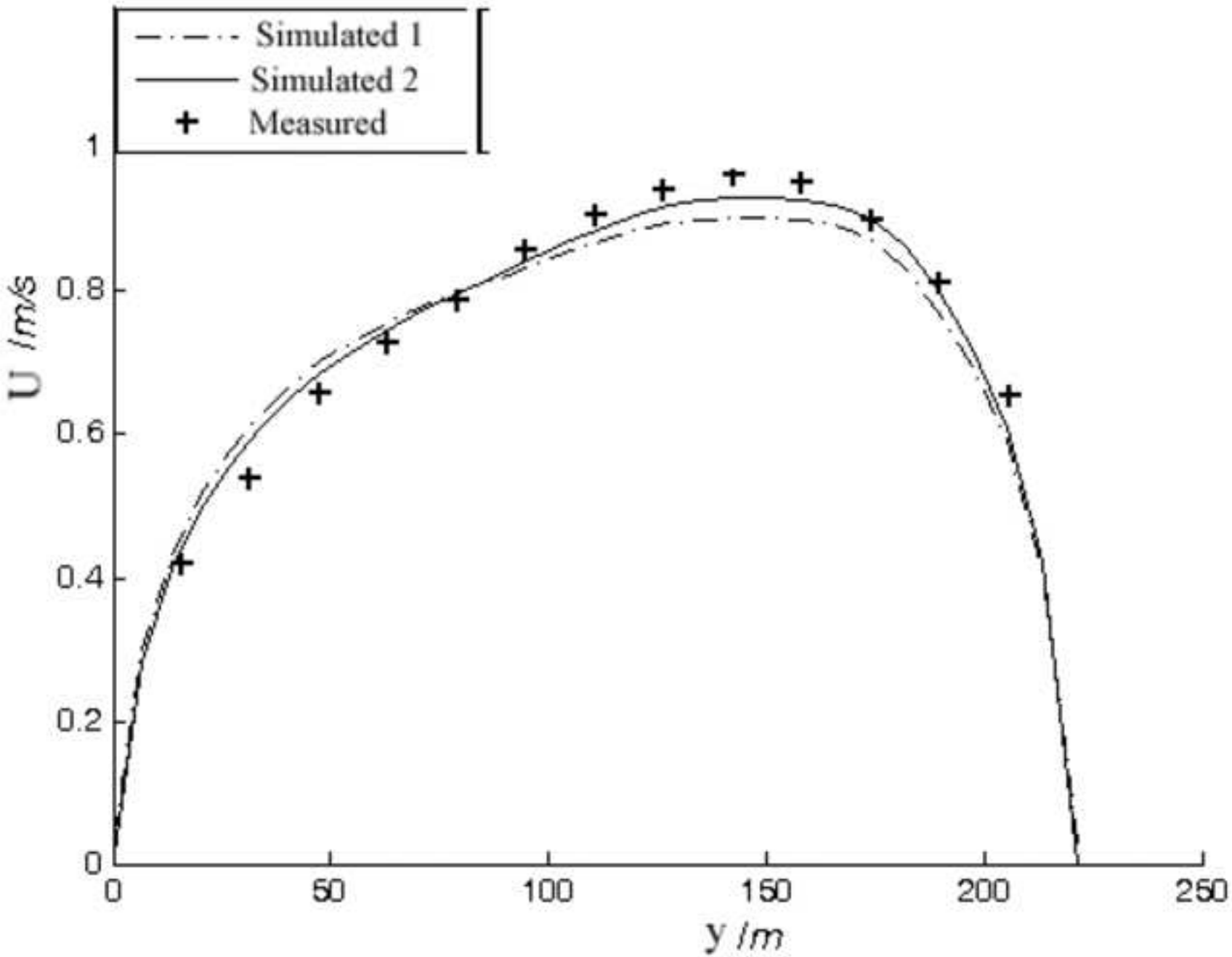

Figure 5(2)
Click here to download high resolution image

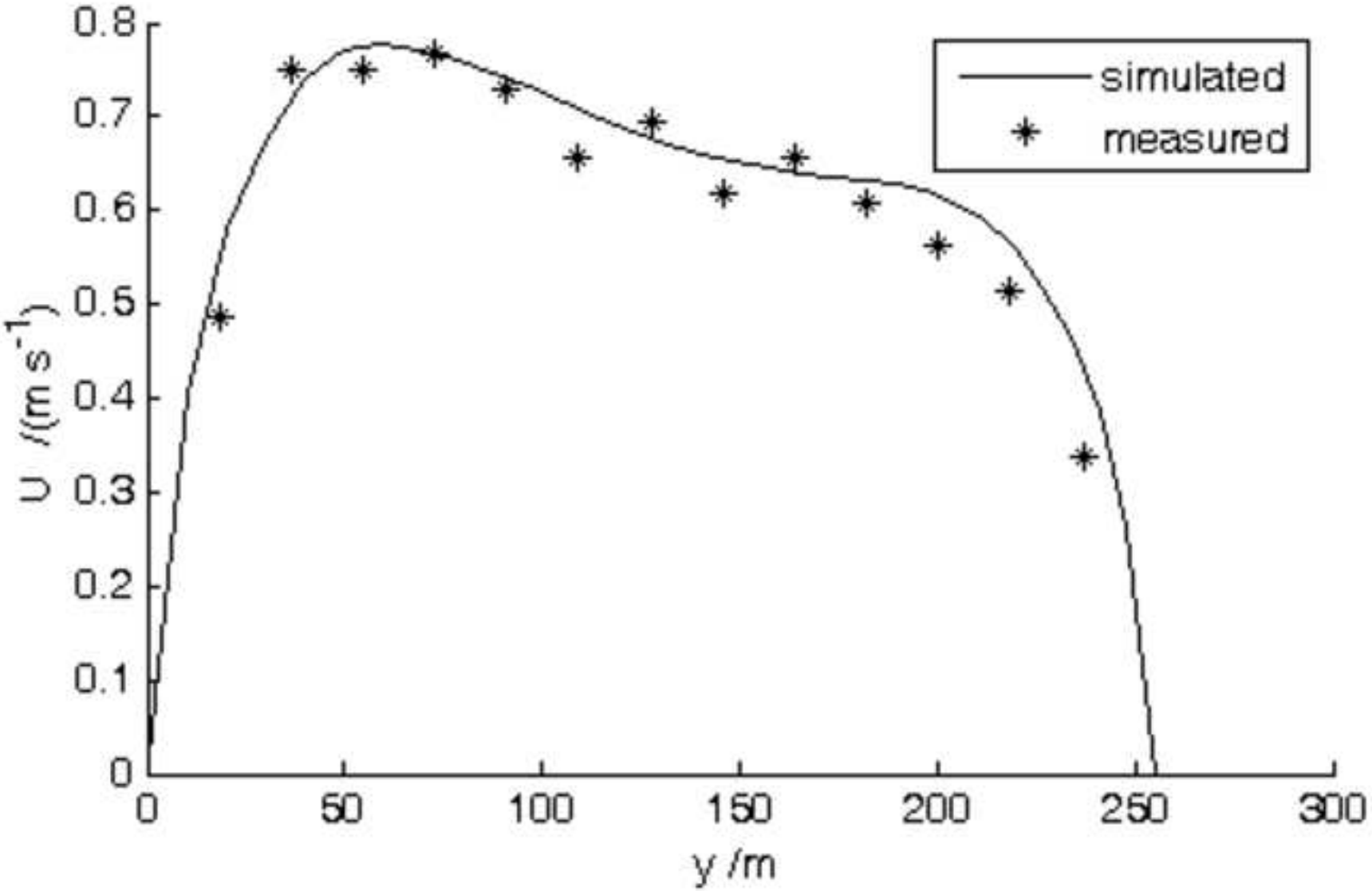

Figure 5(3)
Click here to download high resolution image

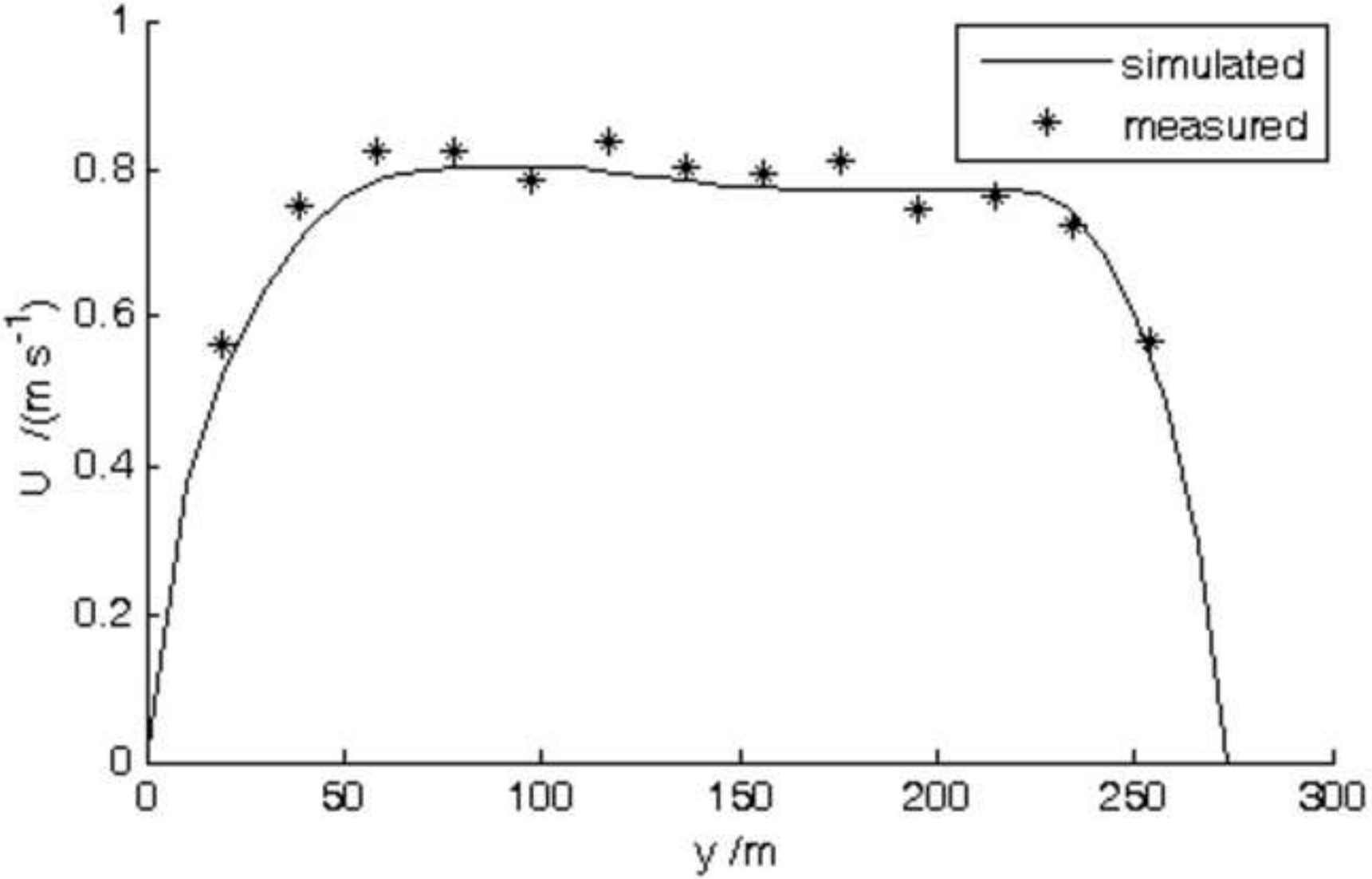

Figure 6

Click here to download high resolution image

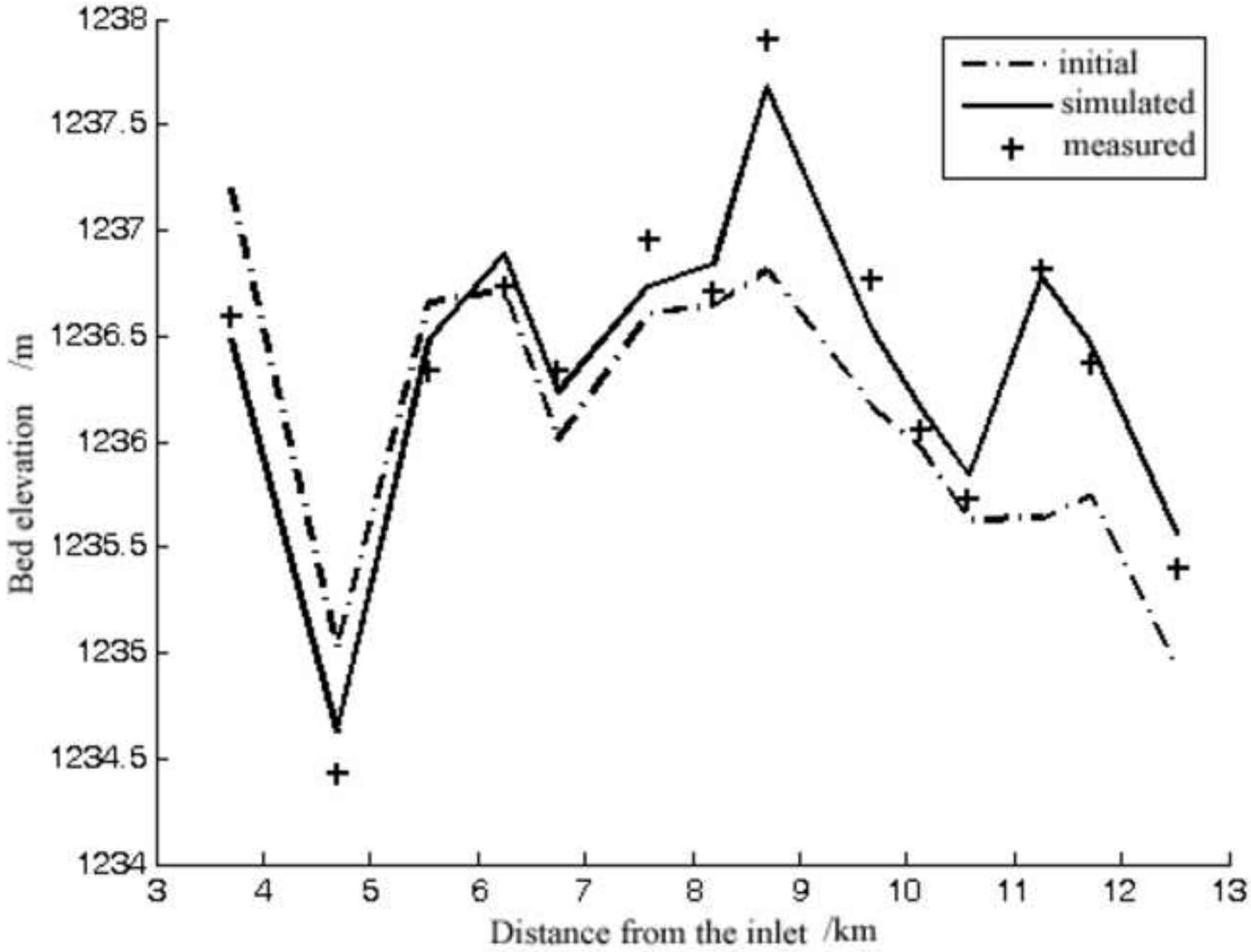

Figure 7(1)
Click here to download high resolution image

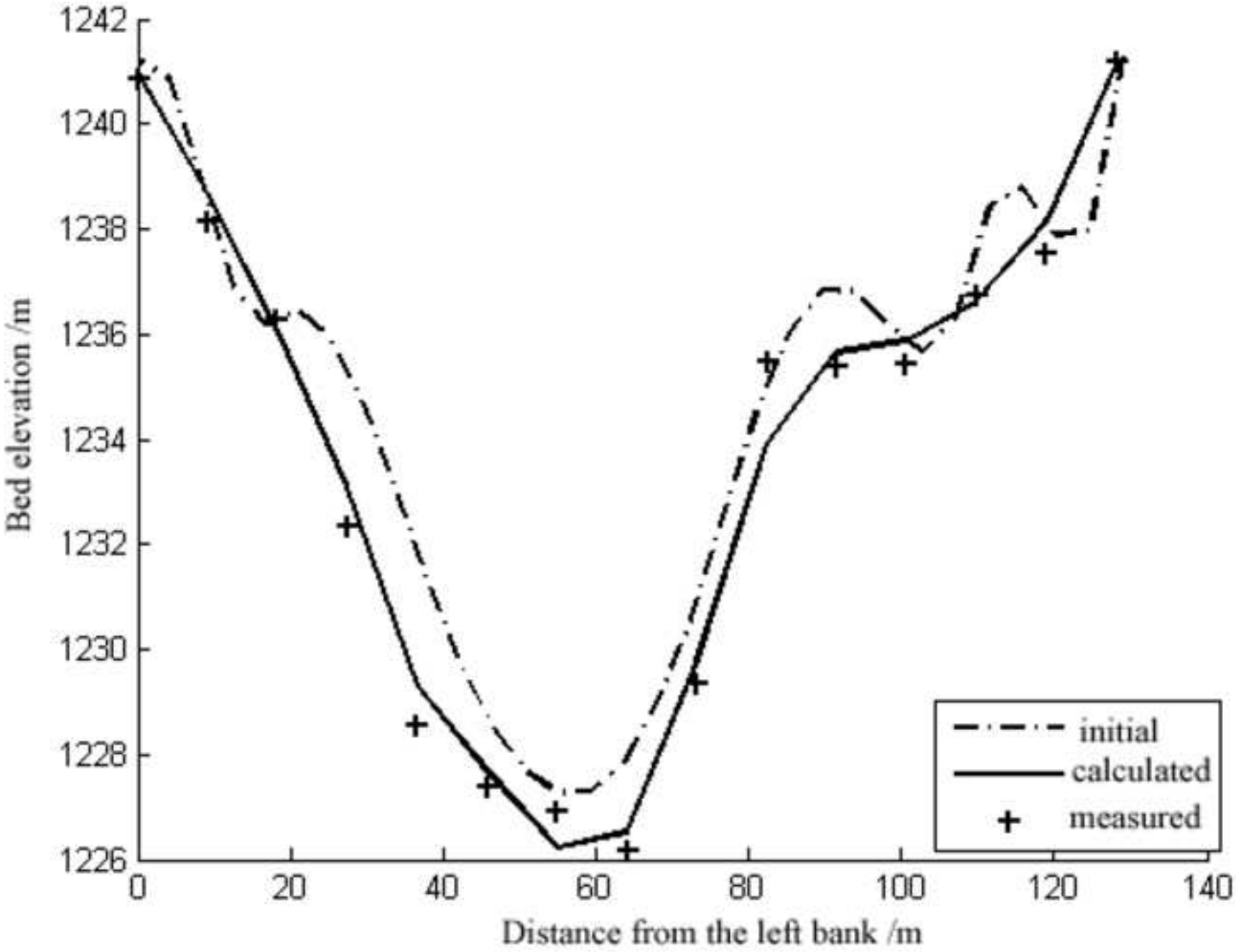

Figure 7(2)
Click here to download high resolution image

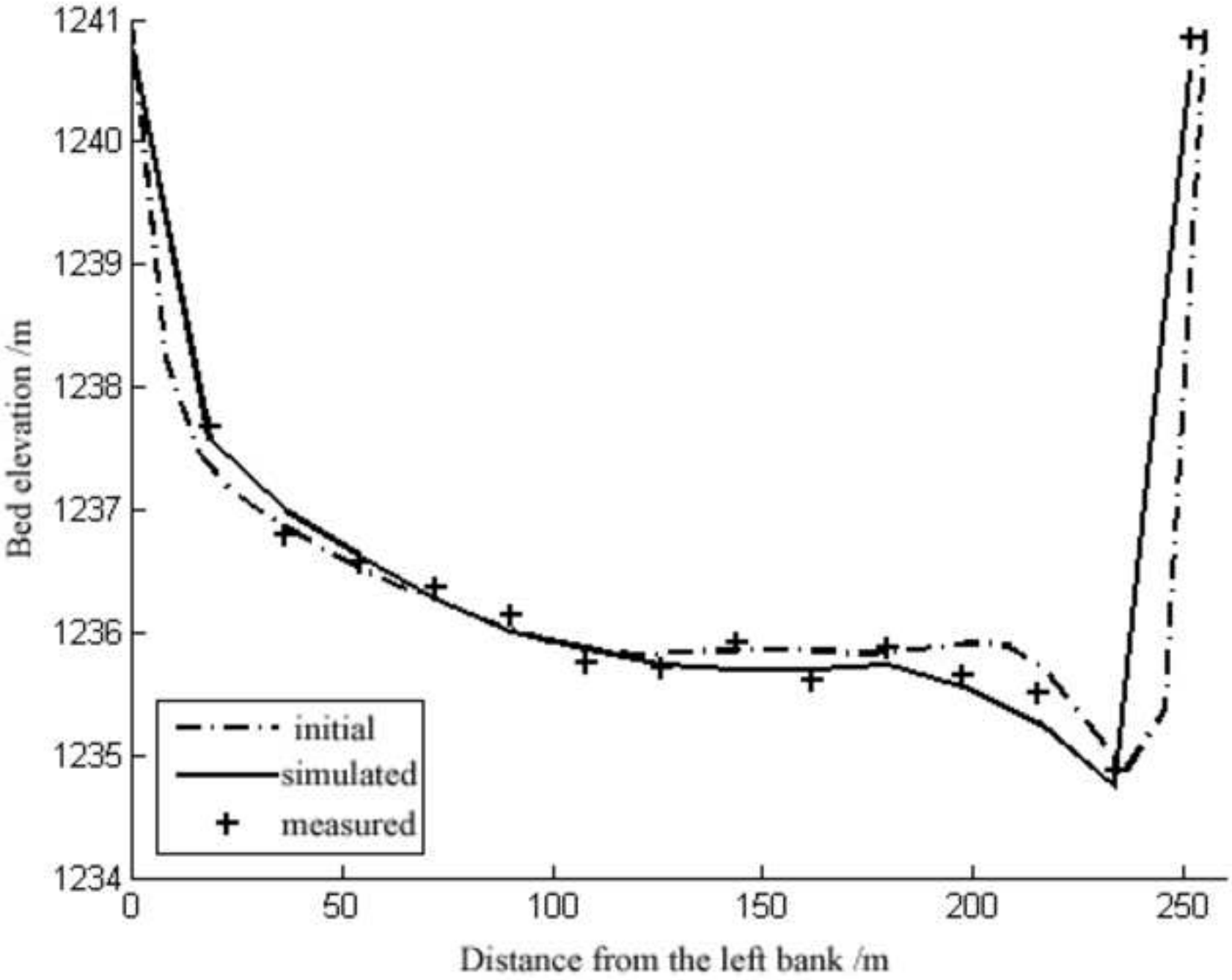

Figure 7(3)
Click here to download high resolution image

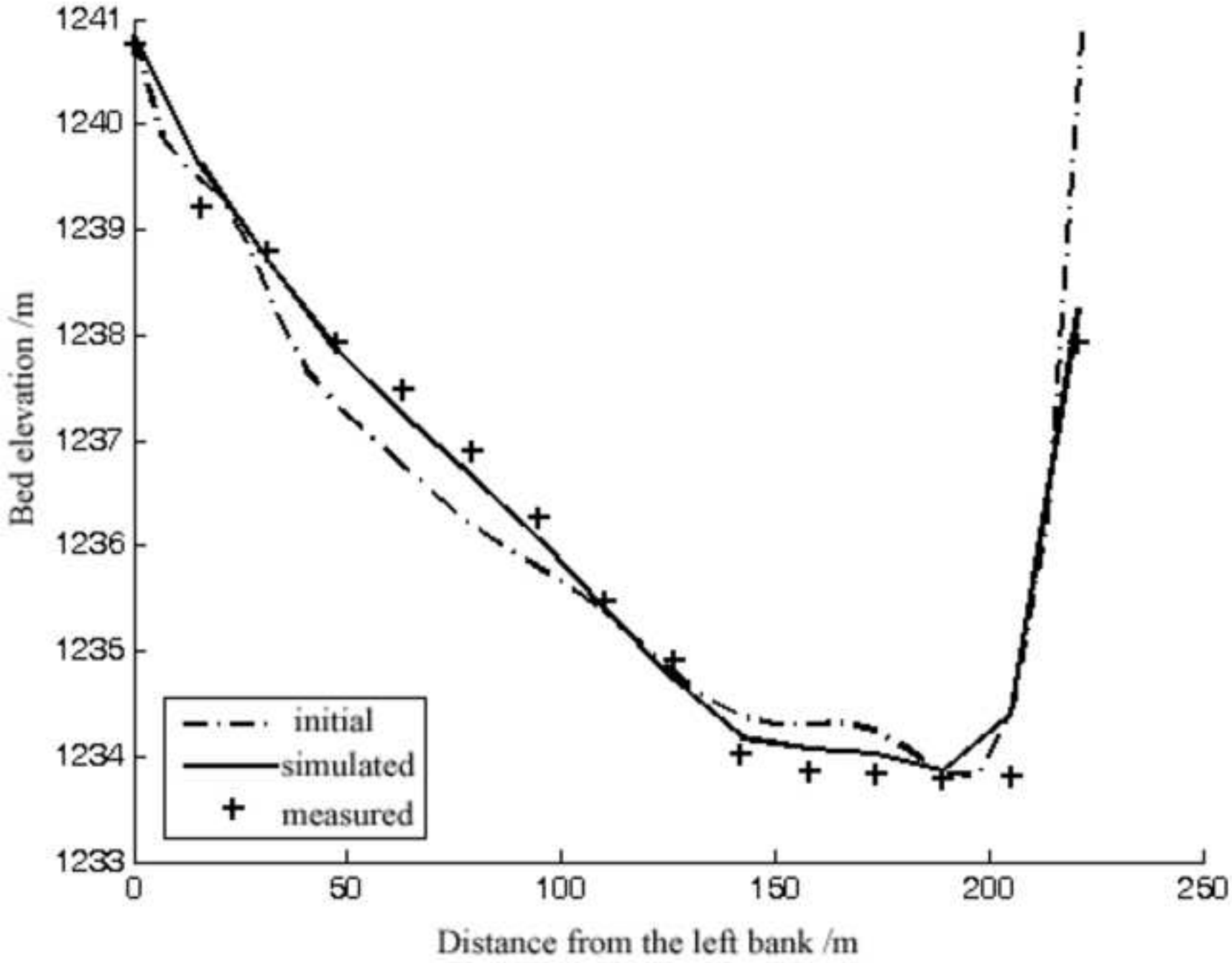

Figure 8

Click here to download high resolution image

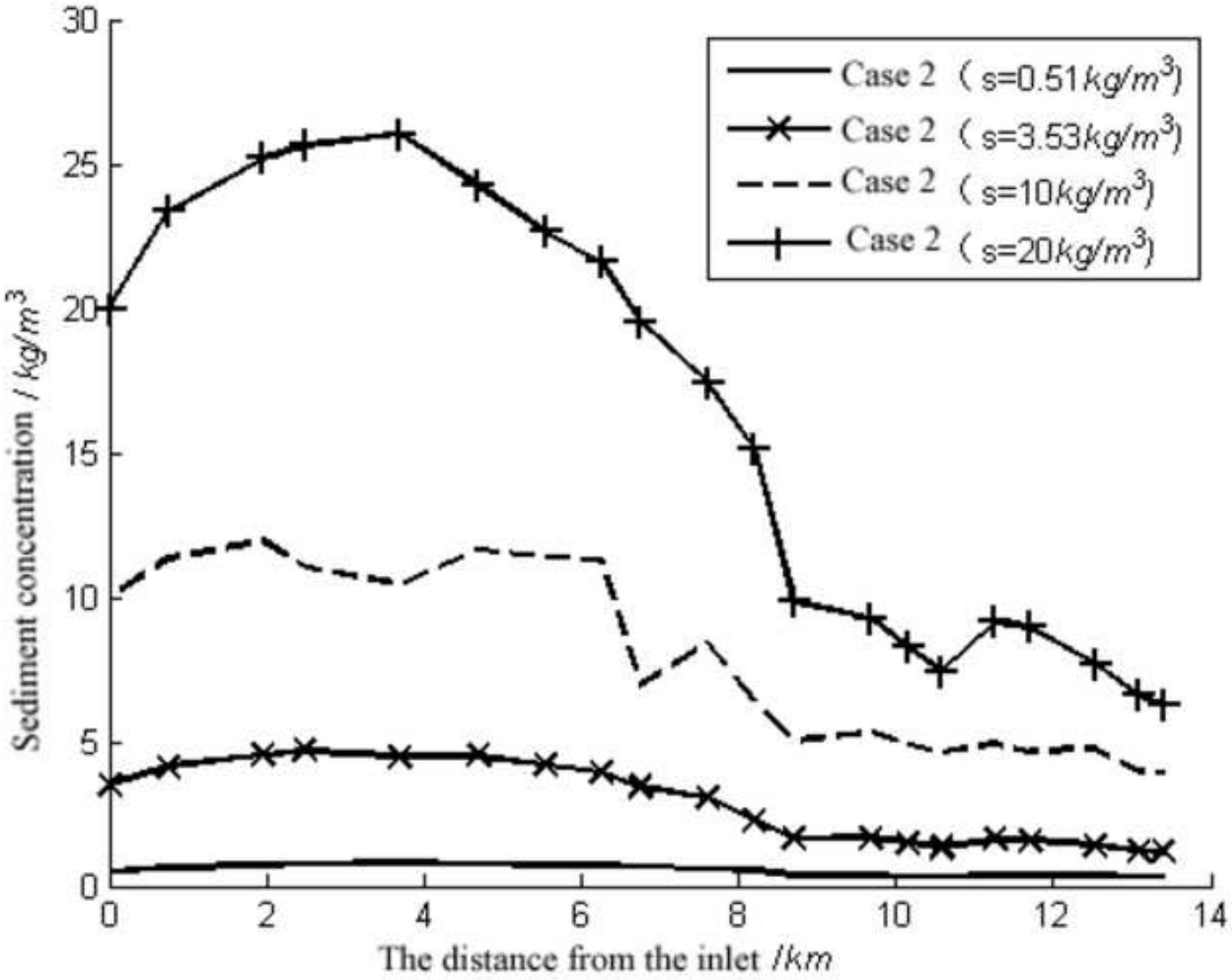

Figure 9

Click here to download high resolution image

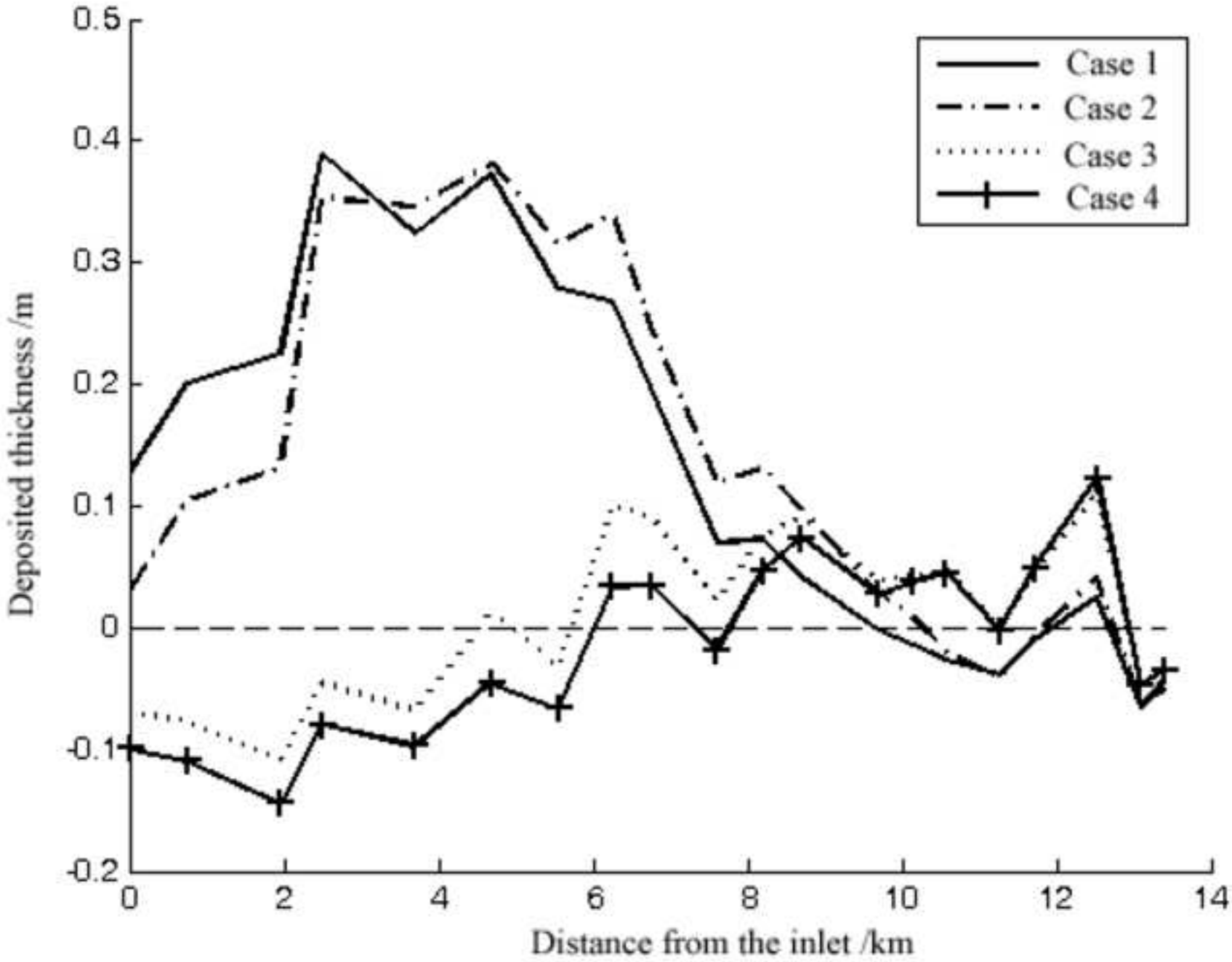

Figure 10
Click here to download high resolution image

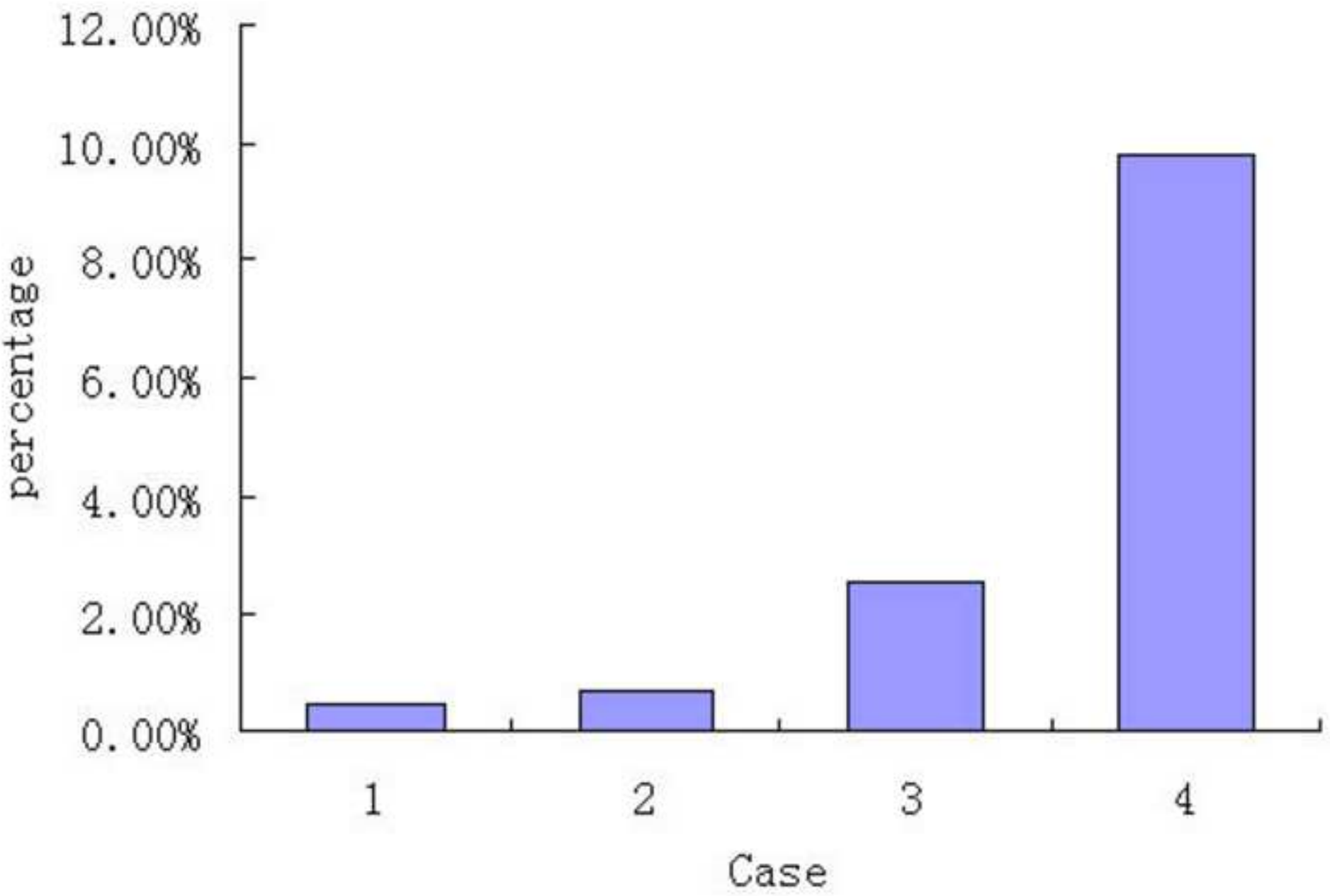

Figure 11(1)
Click here to download high resolution image

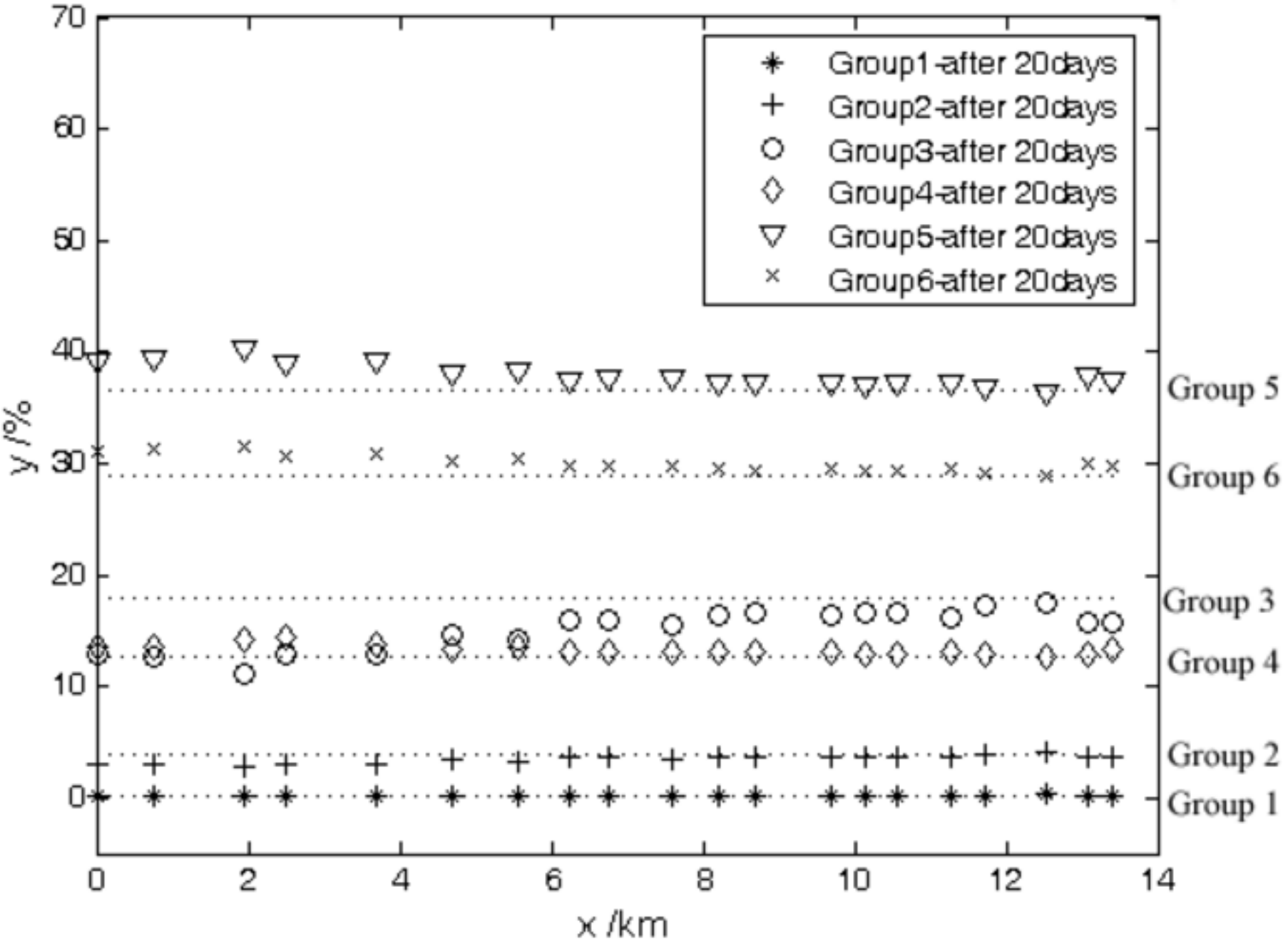

Figure 11(2)
Click here to download high resolution image

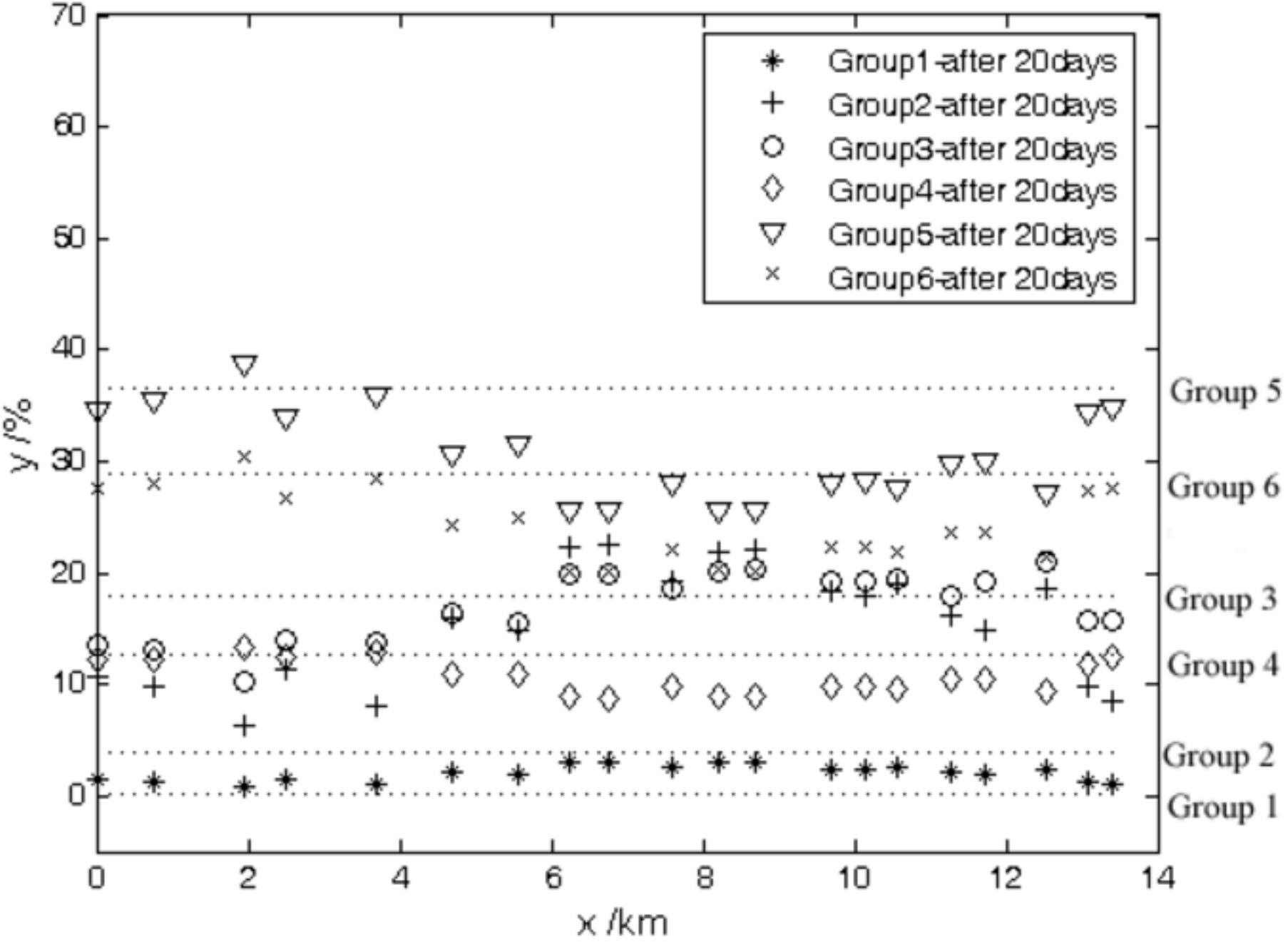

Captions of figures:

Figure 1 The grid and control volume of finite volume method

Figure 2 Meshes distribution near banks and bends

Figure 3 Plane view of Shapotou reservoir(The flow is in from SH15 and out from SH1, and the direction of axis x is consistent with the east)

Figure 4 The distribution of total and group suspended sediment capacities(Case 2)

Figure 5 Comparison of simulated and measured depth averaged velocities on three typical cross-sections

Figure 6 Comparison of simulated and measured bed elevation along the longitudinal direction

Figure 7 Comparison of the measured and the simulated bed elevations on three typical cross sections:（1）SH10（2）SHJ5（3）SH7

Figure 8 Distribution of suspended sediment concentration along the centerline of the studied reach under the condition of Case 2

Figure 9 Comparison of the simulated bed deformations among the four cases with the same sediment concentration（3.53kg/m^3）at the inlet

Figure 10 Percentage of bed deformation caused by bedload sediments in four cases

Figure 11 The variation of effective bed material composition after 20 days:

(1) (a) S_{in}=0.51kg/m^3 (b) S_{in}=10kg/m^3